

A COMPUTATIONAL NEURO-INSPIRED MODEL THAT
GENERATES REALISTIC 3D EYE-HEAD GAZE SHIFTS

Lennaert Wijtze van der Molen

Master Internship Neurophysics

June 2021

Supervisors: prof. dr. A.J. van Opstal and dr. A.D Barsingerhorn
Dept. Biophysics, Donders Centre for Neuroscience.
Radboud Universiteit Nijmegen

Contents

1	Introduction	2
2	Theoretical background	2
2.1	Eye-head gaze shifts	2
2.2	Donders' Law and Listing's Law	5
2.3	Existing models of eye-head gaze control	8
2.3.1	Goossens & van Opstal 1997	8
2.3.2	Tweed 1997	9
2.3.3	Daemi and Crawford 2015	10
2.3.4	van Opstal & Kasap 2018, 2019	10
2.4	Problem statement	11
3	Mathematical methods	12
3.1	3D Rotations: Quaternions	12
3.1.1	Using quaternions to describe rotations	12
3.1.2	Angular velocity/acceleration, orientation, and coordinate velocity/acceleration	13
3.1.3	Using quaternions to describe 3D eye and head orientations	14
4	Model description	15
4.1	SC signal - desired gaze displacement in world coordinates	16
4.2	Desired orientation of the head	16
4.3	Desired eye orientation in the head	17
4.4	Linear eye and head burst generator	18
4.5	VOR	19
4.6	Velocity integration	20
5	Methods	20
5.1	Saccade parameters	20
5.2	Model parameters	21
5.3	Experiment parameters	21
5.3.1	Traces of oblique gaze shifts	21
5.3.2	Consecutive targets	21
5.3.3	Gaze shifts with unaligned initial head and gaze orientations	22
5.3.4	Gaze shifts with random initial orientations and random targets	22
5.3.5	Gaze shifts with centered initial orientations to targets within the OMR	22
6	Results	22
6.1	Traces of oblique gaze shifts	22
6.2	Consecutive targets	24
6.3	Gaze shifts with unaligned initial head and gaze orientation	27
6.4	Trials with random initial orientation and random targets	30
6.5	Gaze shifts to targets within the OMR	33
7	Discussion	34
8	Conclusion	37
9	Data figures	40

1 Introduction

Every waking moment we constantly reorient our eyes with the goal of perceiving the world around us. This task is almost always perceived as effortless and is performed, most of the time unconsciously, more than hundred-thousand times each day. On closer consideration the task seems less trivial, as the eye is attached to the head and the head is attached to the body which is able to move independently. Furthermore, the world itself is also far from static, but directing our eyes at moving targets is also performed with ease. Considered from a computational standpoint, something as simple as looking at a moving car while walking on the street becomes a complex task where 3-dimensional rotations, translations and velocity estimations have to be combined accurately and quickly. The perceived ease of this task is thus in stark contrast with its computational requirements. How the brain computes these reorientations of the eye with respect to the world, called gaze saccades, remains an open question. In this paper we study this question by creating a 3-dimensional neurobiologically plausible computational model that simulates gaze shifts as combined eye and head movements. Most importantly, we incorporated a specific role for a neural structure in the midbrain called the superior colliculus, as recent studies strongly suggest that its firing properties determine the kinematics of gaze saccades[1, 2, 3]. To achieve this we adapted the only 3-dimensional active kinematic model of gaze saccades[4] such that the firing properties of the superior colliculus determined the desired kinematics. Subsequently we found that our model was able to simulate gaze shifts that replicate the kinematics and statistics of gaze shifts in human subjects. Hence we have developed the first 3-dimensional model where the firing properties of the superior colliculus determine the kinematics, thereby showing that it is theoretically possible to devise such a model. This is a potential important contribution to understanding how the brain can solve this complex sensorimotor task. Future work could potentially expand our model to a wider range of natural behaviours, by taking into account the placement and functioning of the ocular muscles and considering dynamic head and body positions.

2 Theoretical background

2.1 Eye-head gaze shifts

Gaze saccades. Gaze is the orientation of the eye with respect to the world. More specifically, it corresponds to the direction of the fovea with respect to the world. The fovea is a small area on the retina with a very high spatial resolution and in the rest of the retina the spatial resolution rapidly decreases with retinal eccentricity. The direction of the fovea is continuously directed towards points of interests in the form of rapid steps, called saccades, in order to obtain a clear visual percept of the world. Saccades have very stereotyped characteristics: Their 2D-trajectories are almost perfectly straight, there is a linear relationship between saccade duration and amplitude, and the peak eye velocity saturates with increasing amplitude. These characteristics are known as the ‘main sequence’ and they imply a nonlinearity in the saccadic system, which we will further discuss below [5].

Superior colliculus. A crucial neural structure for the generation of saccades, which is located in the midbrain is the superior colliculus (SC). The SC acts as a sensorimotor interface, in which sensory target signals are transformed into goals for eye-head motor commands[6]. The SC contains a topographical map of gaze saccades where small saccades are represented rostrally and large saccades caudally[7]. Electrical stimulation of the SC generates normal saccades with a specific size and direction depending on the location in the motor map. Because of these properties, the SC has often been used as a starting point for modelling saccade behaviour. In the classic model, shown in figure 1, the SC encodes a step of the desired eye displacement, ΔE , which is compared with the actual displacement, $\Delta e(t)$, through a local feedback loop to yield a dynamic motor error signal, $me(t)$, which is transformed into an eye velocity signal, $\dot{e}(t)$, by saccadic burst cells that are nonlinear in this model in order to obtain main sequence behaviour.

Saccadic burst generators. The nonlinearity in the saccadic system has often been attributed to the saccadic burst generator which sends a saturating velocity signal to the eye-muscle plant [4, 8, 9, 10, 11]. However, there is no direct evidence that the input-output relationship of the saccadic burst generator causes this saturation. Furthermore, horizontal and vertical velocity profiles need to be linearly scaled versions of each other for oblique saccades to have straight trajectories. If driven independently, this would necessitate for nonlinear horizontal and vertical burst generators to be cross-coupled in a highly complicated manner, for which there is also no direct evidence.

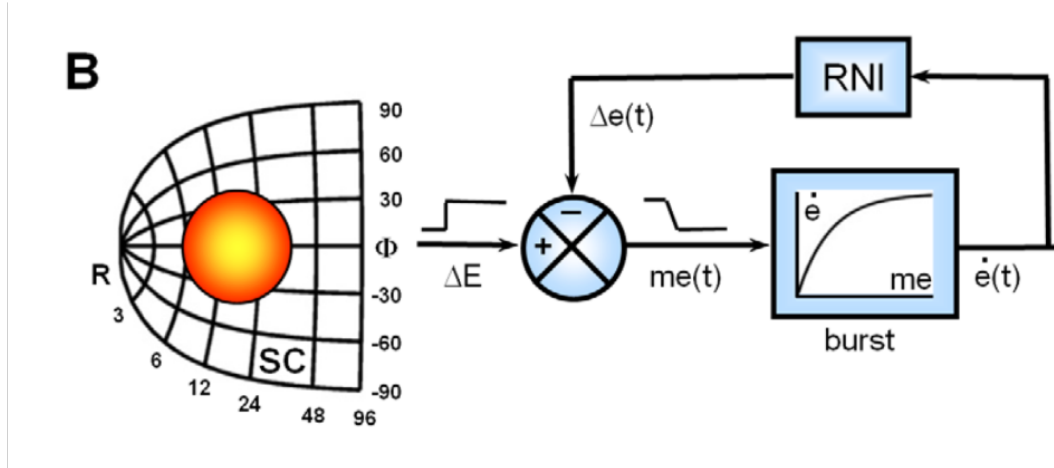


Figure 1: Classic 1D-model of saccade velocity generation[2], after Jürgens et al. [10]. The SC encodes a desired eye displacement in the form of a step, which is compared with the actual displacement through a local feedback loop (called the Resettable Neural Integrator, RNI) to yield a dynamic motor error. A saturating burst generator generates saturating eye velocity signals, resulting in main-sequence behaviour. Plant mechanics transforming eye velocity into position signals and separating horizontal/vertical burst generators are not shown here.

Superior colliculus burst profiles. More recently, the temporal properties of the SC activity patterns have also become a subject of study, which revealed that its firing properties are correlated to the saccade kinematics[1]. Analysis of SC firing profiles and gaze kinematics during blink-perturbed saccades revealed that blinks alter almost every variable related to the saccade and neural activity, except the total number of spikes in the saccade burst and the saccade-endpoint accuracy[1]. This resulted in a novel theory for the role of the SC, in which the total eye displacement is dynamically encoded through the summation of the movement contributions of all individual SC spikes, and the velocity profile is thus governed by the instantaneous firing rate of the population. In this model, the burst generators could be kept linear, since the main sequence properties were completely explained by the firing properties of the SC. Further in-depth analysis of the SC firing properties supported this theory, and showed that the firing properties of the SC vary systematically with the position of cells in the motor map and match eye-velocity profiles remarkably well. The rostral burst profiles of smaller saccades had higher peak firing rates and shorter durations than the caudal burst profiles of larger saccades[2]. The combination of the spatial distribution of spike-effectiveness on the motor system together with their firing rate explains the saturation of peak eye velocity with saccade amplitude. Thus, in this theory the main sequence can completely be explained by the SC firing profile and no longer requires nonlinear burst generators. Since individual SC cells recruited in saccade burst profiles also synchronize their bursts[2], ensuring that the directional information given by the sum of all individual spikes remains constant, straight trajectories for oblique saccades are an emergent property of this theory.

Eye-head coordination. Gaze saccades do not always consist of eye movements only, but are often the combination of precisely coordinated eye and head movements. Electrically stimulating the SC in cats and monkeys while the head was unrestrained resulted in combined eye-head gaze shifts[12][13]. Stimulating the same site resulted in gaze shifts of equal size, but relative contributions of the eye and head varied depending on the initial eye-in-head position. This suggests that both the eye and the head are commonly driven by the SC signal which encodes not only the eye movement but the total gaze displacement, ΔG .

Vestibular system. The eye is located in the head, causing the orientation of the eye with respect to the world to change if the head is moving. However, while fixating your gaze at a point on the wall and simultaneously moving your head it can be noted that stabilizing gaze with respect to the world is surprisingly easy. This is the result of a reflex in which angular head velocity is measured by the semicircular canals of the vestibular organ in the inner ear[14], resulting in the vestibulo-ocular reflex (VOR) by driving an equal but oppositely directed eye-angular velocity[15]. This reflex ensures stable vision with respect to the world when the head is making expected or unexpected passive movements. However, during gaze shifts the VOR is turned off in the direction of the gaze shift until the target is foveated in order to allow the eye to move in the direction of the intended gaze shift as quickly as possible[16]. As a result, even a simple horizontal gaze shift already has complex dynamics with a lot of room for variability, as shown in figure 2. For example, the onsets of the eye and head movements can differ, which will result in varying eye and head contributions to the overall gaze shift. Furthermore, the head often continues to move after gaze has fixated the target, at which moment the VOR becomes fully functional to stabilize the direction of gaze in space by rotating the eye in the opposite direction. As a result, the relative eye and head contributions during the gaze shift usually differ substantially from the final displacements at the end of movement. Despite an infinite amount of possible eye and head contributions, movement strategies for specific initial conditions are highly reproducible, and have been suggested to reflect of a form of optimal control[17].

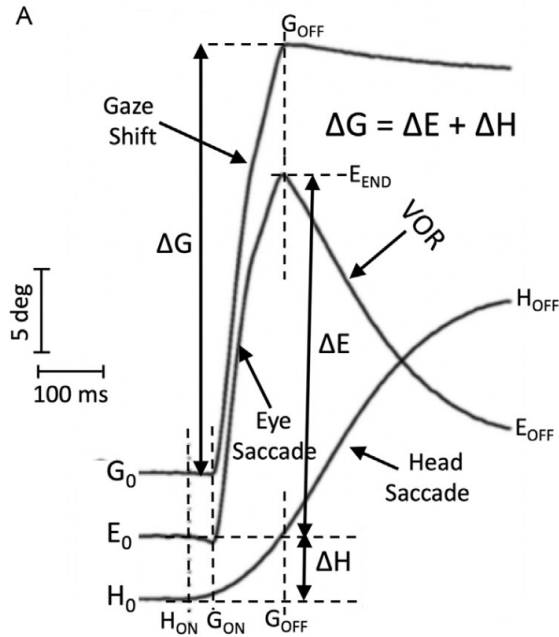
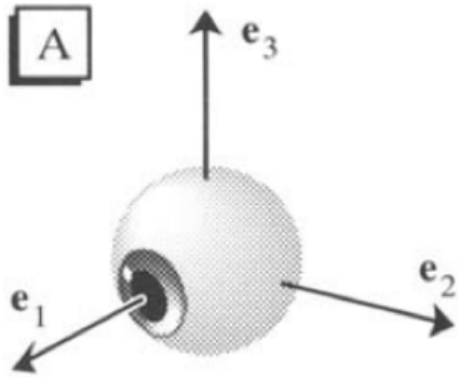


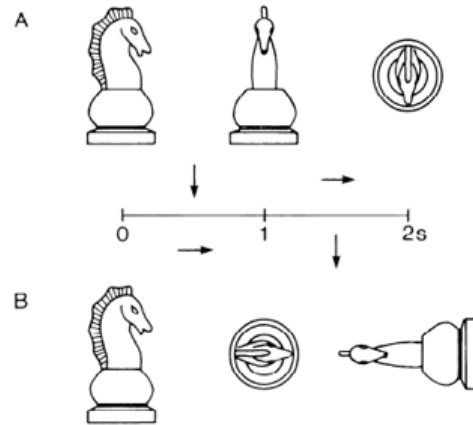
Figure 2: Example of a one-dimensional gaze shift to an auditory target, reproduced from Van Opstal et al.[3]. Initial orientations are aligned but shifted on the graph to better illustrate separate movement tracks. The gaze shift ΔG is defined between the onset and offset (G_{ON} / G_{OFF}) of gaze movement and the relative contributions of eye and head movement, ΔE and ΔH , are measured during this period. After the gaze shift, the head continues to move towards the target and the VOR causes the eye to counter-rotate with equal velocity. Onset of movement varies between trials. In this example, onset of head movement is earlier than onset of eye movement.

2.2 Donders' Law and Listing's Law

The goal of a gaze shift is to point the fovea at a target, which requires only 2 degrees of freedom: a desired horizontal and vertical orientation. This leaves the third coordinate, rotation about the line of sight, or 'cyclo-torsion' (see figure 3a), unspecified by the task. Three-dimensional rotations require special attention because, unlike 1-dimensional rotations, they are non-commutative. This means that the order of rotations influences the final orientation, as illustrated in figure 3b. Furthermore, random consecutive rotations will generally always result in an accumulation of torsion[18]. In theory, any amount of torsion would still allow the fovea to point at the target if limiting mechanical constraints such as eye-muscles are ignored. It is thus interesting to see what strategies the oculomotor system incorporates to deal with these 3-dimensional properties and whether accumulation of torsion occurs after consecutive saccades.



(a) Figure from Haslwanter[19]. Three rotation axes of the eye in a right handed coordinate system. e_1 is the torsional axis unit vector, describing rotation about the line of sight. e_2 is the horizontal axis unit vector, describing vertical rotation. e_3 is the vertical axis unit vector, describing horizontal rotation.



(b) Figure from Tweed[18]. Two chess pieces starting in the same initial orientation are rotated with two identical consecutive rotations in differing order. The final orientations are not identical, illustrating that 3-dimensional rotations are non-commutative.

The Dutch physician Franciscus Donders found that accumulation of torsion does not occur and that the eye will assume a unique 3-dimensional orientation for any specific gaze direction[20], a result that is called Donders' law. Measurements of ocular torsion during saccades reveal a deliberate strategy, as shown in figure 4. This figure shows the 3-dimensional orientation of the eye under head-fixed conditions. The torsional rotation components of the eye in the head, in essence how much the eye has rotated about its line of sight, lie in a 2-dimensional plane that is tilted with respect to looking straight ahead[21]. The orientation orthogonal to this plane ('orientation' in figure 4) is often called the primary position and under head-fixed conditions any 3-dimensional orientation of the eye is orthogonal to this primary direction. In other words, ocular torsion or rotation about the line of sight is always zero with respect to the primary position. This result is called Listing's law and is a more specific formulation of Donders' law in which the amount of ocular torsion for each direction is specified to be zero with respect to the primary position. The 3-dimensional orientation of the head when freely looking around also seems to follow a form of Donders' law in which the torsional component is a function of the horizontal and vertical components that is non-zero except for the primary position[22][23]. However, unlike eye movements, any 3-dimensional orientation of the head within the physical limits of the body can voluntarily be obtained prior to or during a gaze saccade[24].

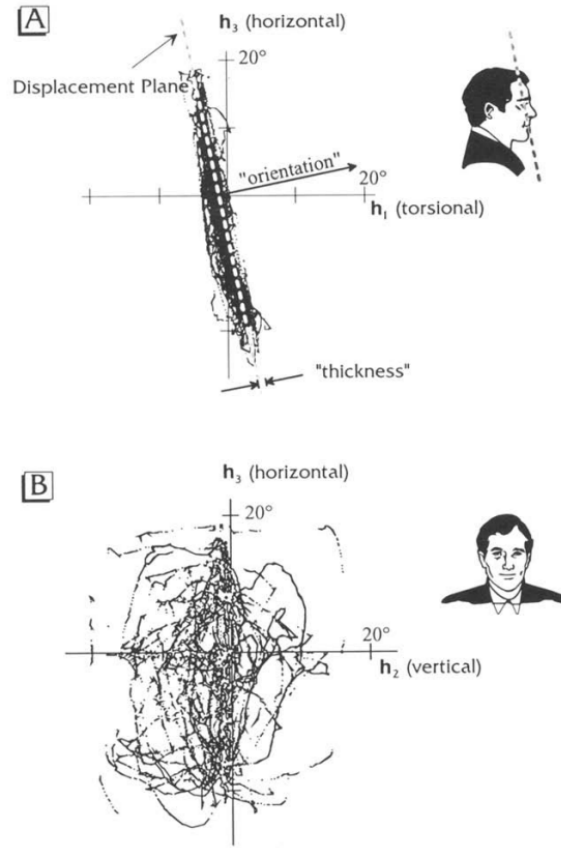


Figure 4: Figure from Haslwanter[19]. Side (A) and front (B) view with respect to looking straight ahead of eye rotation vectors of a subject freely looking around a room. Only end points of saccades are plotted.

The implementation of Listing's law for the oculomotor system is highly non-trivial. In order to get from one orientation of the eye to the next, an infinite amount of rotations are possible that would get the fovea to look at the target. However, the one specific rotation that does not result in an accumulation of torsion is consistently executed. This can not be the result of chance and indicates the presence of a deliberate mechanism. How this mechanism is implemented has been the subject of much debate where two distinct options have been considered in detail. The first option is that Listing's law is entirely mechanically implemented through a pulley-like system at the level of the eye-muscles that automatically prevents torsion from accumulating[25]. The second option is that Listing's law is neurally implemented and that specific velocity signals are generated such that saccades follow Listing's law. Although both options merit consideration, we motivate that Listing's law is implemented neurally. Firstly, the eye violates Listing's law during head-free gaze shifts and returns to Listing's plane only at the end of the movement[26][27], indicating that saccades have three degrees of freedom. Secondly, electrically induced ocular torsion in monkeys does not transiently drift back but is instead corrected during the subsequent saccade[28]. The rotation that returns the eye to Listing's plane would under normal circumstances have resulted in accumulation of torsion, which suggests that the oculomotor system chooses not to implement rotations that violate Listing's law, even though they are possible. These findings are better explained by a neural implementation of Listing's law and we will therefore implement this in our model.

2.3 Existing models of eye-head gaze control

2.3.1 Goossens & van Opstal 1997

The head can freely rotate on the neck and the eye can freely rotate in the head. The direction of gaze is, in 2D, the sum of the direction of the eye and the head and thus the direction of the eye and the head do not necessarily coincide. As a result, the direction of the target with respect to the head (head error) and the direction of the target with respect to the eye (gaze error) do not always coincide. This is illustrated in figure 5.

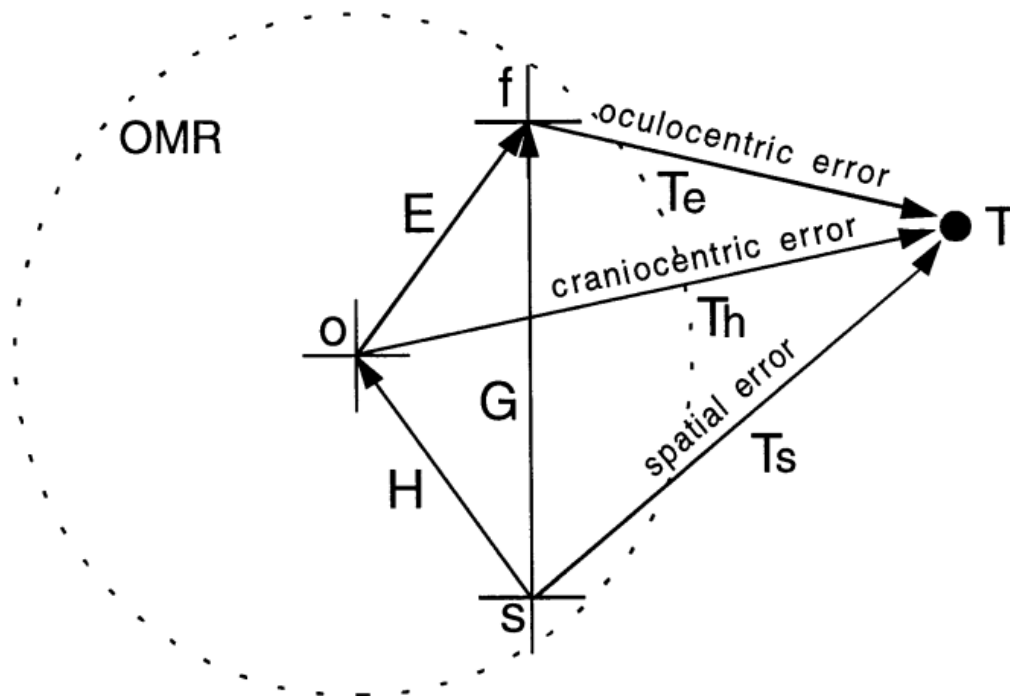


Figure 5: Figure taken from Goossens and Van Opstal illustrating in 2D the different reference frames of the eye (oculocentric), head (craniocentric) and gaze (spatial or bodycentric) [1]. Here, s is the center of the body (spatial frame), o is the center of the oculomotor range and f is the fixation point of the fovea. \mathbf{H} is the direction of the head in space, \mathbf{E} is the direction of the eye in the head and \mathbf{G} is the direction of the eye in space, or gaze. With \mathbf{T} being the direction of the target, we get three different errors with respect to each reference frame: \mathbf{T}_s is spatial error giving the direction of the target in space, \mathbf{T}_h is the craniocentric or head error, \mathbf{T}_e is the oculocentric or gaze error. From the figure multiple reference frame transformations can be obtained: $\mathbf{G} = \mathbf{H} + \mathbf{E}$, $\mathbf{T}_h = \mathbf{E} + \mathbf{T}_e$ and $\mathbf{T}_s = \mathbf{H} + \mathbf{T}_h = \mathbf{H} + \mathbf{E} + \mathbf{T}_e$. Note that, as f and o do not coincide, the eye and the head in this example are unaligned.

In their 1997 paper Goossens and Van Opstal studied how the saccadic system deals with these different reference frames and asked whether head movements in a gaze shift are directed towards the initial gaze error or towards the initial head error [8]. For a visual target, the initial error on the fovea is the gaze error. If head movement would be directed towards the initial head error, the brain would first need to perform a coordinate transformation of the initial gaze error from the oculocentric reference frame to the craniocentric reference frame in order to determine the desired direction of the head. In 2D, this is done by adding the initial orientation of the eye to the initial gaze error,

$\mathbf{E} + \mathbf{T}_e$ (see figure 5). Goossens and Van Opstal performed experiments where gaze saccades had to be performed and the head was free to move. The initial orientations of the eye and the head were either aligned or unaligned (in figure 5 they were unaligned) to assess if the direction of head movement was better predicted by the initial gaze error (\mathbf{T}_e) or by the initial head error (\mathbf{T}_h). These measurements revealed that the direction of head movement was better predicted by the initial head error than the initial gaze error. As both eye and head movements are driven by the same desired gaze shift signal from the SC this would require a coordinate transformation of the gaze shift signal into craniocentric coordinates, by adding the initial eye position to desired gaze shift signal. Based on these measurements Goossens and Van Opstal proposed a 2D control theory model in which eye and head movements were both driven by a desired gaze displacement which was subsequently transformed from an oculocentric into a craniocentric reference frame by adding the position of the eye (see figure 5). In 2D, this model explained the behaviour of eye and head movements in human subjects very well. The eye- and head-burst generators in this model were both assumed to be nonlinear in order to simulate nonlinear main-sequence behaviour. The model did not specify an explicit role for the superior colliculus.

2.3.2 Tweed 1997

In 1997 Tweed published the first 3-dimensional model of gaze saccades with combined eye and head movements using quaternions, which will be explained further below [4]. The model has no explicit role for the SC but assumes that the signal that is encoded by the build-up cells in the SC is the direction of the target relative to the eye, the initial gaze error \mathbf{T}_e in figure 5. The oculocentric direction of the target is rotated into a bodycentric direction to obtain the spatial error \mathbf{T}_s , from which desired orientation for the eye and the head are derived that fit Listing's and Donders' law. Firstly, the desired orientation of the head, q_h^* , was defined as a fraction of the spatial error \mathbf{T}_s to fit Donders' law and is not based on the head error \mathbf{T}_h , in contrast to Goossens & van Opstal's model. The desired orientation of the eye was then defined as the orientation of the eye that does not have torsion, and this brings gaze precisely on target when combined with the desired orientation of the head. The 3D mathematics required to perform this coordination transformation will be discussed further below, but the 2D equivalent in figure 5 would be to subtract \mathbf{H}_{DES} from \mathbf{T}_s in order to obtain the desired direction of the eye \mathbf{E}_{DES} : $\mathbf{E}_{DES} = \mathbf{T}_s - \mathbf{H}_{DES}$. The gaze is then given by the sum of the direction of the head and the eye $\mathbf{H} + \mathbf{E}$. In the Tweed model, the final desired orientations of the head and the eye in the head were used to obtain the desired orientation of the eye in space, q_{es}^* . In the 2D analogy, this would be $\mathbf{G}_{DES} = \mathbf{H}_{DES} + \mathbf{E}_{DES}$. The trick used in the Tweed model was to not aim the eye in the direction of the final desired orientation of the eye, but at the current desired orientation of the eye, q_{eh}^+ that would bring gaze on target with respect to the current orientation of the head. In the 2D analogy this is found by subtracting the current direction of the head from the final desired direction of gaze: $\mathbf{E}_{DES(CURRENT)} = \mathbf{G}_{DES} - \mathbf{H}$. Consequently, the gaze was quickly brought on target, and the eye would reach the desired direction as soon as $\mathbf{H} = \mathbf{H}_{DES}$. In 3D the consequence was that the eye ended up in Listing's plane precisely as the head stopped moving and the VOR no longer contributed, as is the case in human subjects[16]. This model predicts large deviations of the eye-in-the-head orientation from Listing's plane for gaze shifts that include torsional head movements, which was confirmed experimentally [29]. The burst generators in this model were also assumed to be nonlinear and generated saturating velocity signals in order to simulate nonlinear main sequence behaviour.

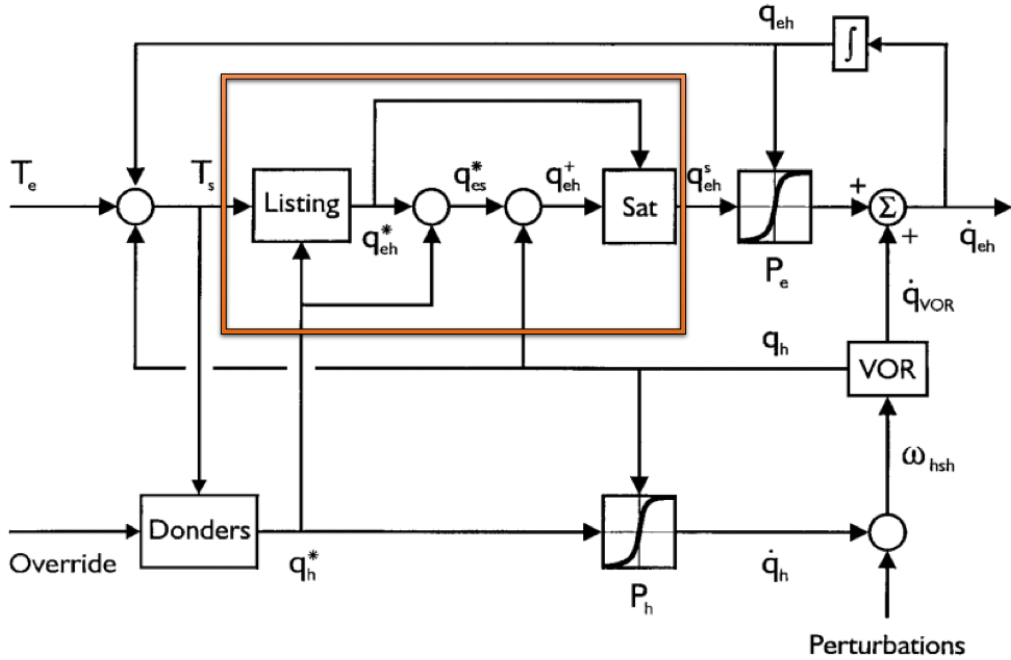


Figure 6: Figure of the '97 3D Tweed model[4]. An oculocentric direction of the target T_e is rotated using the orientation of the eye and the head in to a body-centric direction of the target T_s . Using the Donders and Listing boxes 3D orientations of the eye and the head are fitted such that they conform to Donders' and Listing's Law and the gaze ends up in the direction of T_s . The orange box highlighting the transformation of the desired direction in space in to an oculomotor range (OMR) saturated desired eye orientation that fits Listing's plane when the head stops moving is used in reference to figure 7.

2.3.3 Daemi and Crawford 2015

In 2015 Daemi and Crawford published the second 3D model of head-free gaze shifts [30]. The model is a static kinematic model and mainly concerns the derivation of desired orientations and not the neurobiological origins of the underlying kinematics, which is the main focus of our study. It therefore falls outside the scope of this paper.

2.3.4 van Opstal & Kasap 2018, 2019

Van Opstal and Kasap published a 2-dimensional model that adapts the Goossens 1997 model by giving an explicit role to the SC in which the saccade kinematics are encoded through the SC firing rates and where the total cumulative sum of spikes of the recruited population encodes the desired gaze displacement trajectory[3]. In this model, the main-sequence behaviour was fully explained by the firing properties of the SC and as a result the burst generators were assumed to be linear. Experiments described in the paper also showed further eye-position dependent movement strategies and kinematics. Delays of head movements were longer, gaze velocities were lower and durations were longer for gaze shifts where the eye is limited by the oculomotor range (OMR), in contrast to gaze shifts where the eye was not limited by the OMR. Further, SC burst profiles had lower peak firing rates and longer burst durations during gaze shifts where the eye was limited by the OMR, in line with the theory that the SC determines saccade kinematics.

2.4 Problem statement

The goal of our current study is to create a 3D model that simulates realistic gaze shifts as combined eye and head movements where the SC signal encodes the desired gaze velocity and the SC firing properties explain saccade kinematics like the main sequence while the velocity burst generators remain linear. Final orientations of the eye and the head are to be determined by Listing's and Donders' law and are to be implemented neurally downstream from the SC. Saccade kinematics and statistics should resemble data from human subjects.

3 Mathematical methods

3.1 3D Rotations: Quaternions

Quaternions are 4-dimensional mathematical objects that are often used to describe 3-dimensional fixed-axis rotations and rigid body orientations. A quaternion consists of a complex vectorial 3-dimensional term, analogous to the axis of rotation, and a real scalar term. Their mathematical properties suit the description of rotational kinematics very well. The goal of this model is not to explain the mathematics of quaternions and how they differ from methods like using Euler angles, more info on this can be found for example here [19]. Below, only their notation and use in this paper are described.

3.1.1 Using quaternions to describe rotations

A quaternion is defined as follows :

$$q \equiv q_0 + q_x \hat{\mathbf{i}} + q_y \hat{\mathbf{j}} + q_z \hat{\mathbf{k}} \quad (1)$$

where q_0 is the scalar part, the contributions to the vectorial part, $\mathbf{q} = (q_x, q_y, q_z)$ and the complex unit vector $\mathbf{I} \equiv (\hat{\mathbf{i}}, \hat{\mathbf{j}}, \hat{\mathbf{k}})$ of the (forward-pointing) torsional x-axis, the (leftward pointing) horizontal y-axis and (upward-pointing) vertical z-axis, respectively, with the properties: $\hat{\mathbf{i}}^2 = \hat{\mathbf{j}}^2 = \hat{\mathbf{k}}^2 = \hat{\mathbf{i}} \bullet \hat{\mathbf{j}} \bullet \hat{\mathbf{k}} = -1$. All quaternions in this paper are unit quaternions, meaning that their norm is 1:

$$|q| \equiv \sqrt{q_0^2 + q_x^2 + q_y^2 + q_z^2} = 1 \quad (2)$$

A unit quaternion describing a rotation around a certain axis \mathbf{n} of θ degrees can therefore be parametrized as follows:

$$q = (\cos(\theta/2) + \sin(\theta/2)(\hat{\mathbf{n}} \bullet \mathbf{I}) \equiv q(\hat{\mathbf{n}}, \theta) \quad (3)$$

The inverse quaternion, q^{-1} corresponds to the complex conjugate of q ,

$$q^{-1} = (\cos(\theta/2) - \sin(\theta/2)(\hat{\mathbf{n}} \bullet \mathbf{I}) = q(\hat{\mathbf{n}}, -\theta) \quad (4)$$

for which the following relation holds:

$$qq^{-1} = q^{-1}q = 1 \quad (5)$$

Finally, the quaternion product, which describes the result of rotation q followed by another rotation p , is computed as:

$$r \equiv pq = p_0q_0 - \mathbf{p} \bullet \mathbf{q} + [q_0\mathbf{p} + p_0\mathbf{q} + \mathbf{p} \times \mathbf{q}] \bullet \mathbf{I} \quad (6)$$

which is again a quaternion, as quaternions form a group. Here, \bullet represents the dot product, and \times the cross product of vectors. Note that, in general, $pq \neq qp$, which is due to the noncommutative property of 3D rotations (commutativity only holds when the rotation axes of the quaternions are parallel).

In this paper, quaternions are used to rotate vectors that correspond to changes in eye-, head- and gaze-orientations. In general, when a vector, \mathbf{v} is rotated about an axis $\hat{\mathbf{n}}$ over an angle θ , the result is given as:

$$\mathbf{v}' = q(\hat{\mathbf{n}}, \theta)\mathbf{v}q^{-1}(\hat{\mathbf{n}}, \theta) \quad (7)$$

As an example, suppose that we rotate the unit vector $\hat{\mathbf{T}} = [1, 0, 0]$, which points straight ahead in the positive x-direction, by 10° 's downward. This corresponds to a positive rotation (right-hand rule) around the horizontal y-axis, which means that the quaternion describing this rotation equals:

$$q(\hat{\mathbf{y}}, 10\pi/180) = \cos(5\pi/180) + \sin(5\pi/180)\hat{\mathbf{j}} \quad (8)$$

Applying the quaternion product to vector \mathbf{T} then yields the following result:

$$\begin{aligned}
\mathbf{T}' &= q\mathbf{T}q^{-1} = (\cos(0.087) + \sin(0.087)\hat{\mathbf{j}}) \cdot \hat{\mathbf{i}} \cdot (\cos(0.087) - \sin(0.087)\hat{\mathbf{j}}) \\
&= (\cos(0.087)\hat{\mathbf{i}} - \sin(0.087)\hat{\mathbf{k}}) \cdot (\cos(0.087) - \sin(0.087)\hat{\mathbf{j}}) \\
&= (\cos(0.087)^2 - \sin(0.087)^2)\hat{\mathbf{i}} - 2\cos(0.087)\sin(0.087)\hat{\mathbf{k}} \\
&= [0.9849, 0, -0.1731]
\end{aligned} \tag{9}$$

This indeed lies in the xz plane. Note that in this example, q describes both a fixed-axis rotation, and an orientation with respect to the unit vector $\hat{\mathbf{T}}$ (which is considered to coincide with the primary position, and therefore is expressed by $q = 0$).

3.1.2 Angular velocity/acceleration, orientation, and coordinate velocity/acceleration

Angular velocity is the measure of how fast a certain object rotates around a certain point. If we use the example of the vector $\mathbf{T} = [1, 0, 0]$ rotating 10° 's downward around the positive y-axis in 1 second, the angular velocity would be:

$$\omega = \frac{10\pi}{180} \frac{1}{s} \hat{\mathbf{y}} \tag{10}$$

If we consider $q(t)$ to be the quaternion describing the instantaneous orientation of the vector \mathbf{T} with respect to the unit vector $\hat{\mathbf{T}} = [1, 0, 0]$, the angular velocity will cause the orientation $q(t)$ to change over time. This is called the coordinate velocity and in the case of quaternions is indicated by $\frac{dq}{dt} = \dot{q}$. A crucial property of 3D rotations is that different orders of consecutive finite rotations result in different orientations, unless the axes of rotation are exactly parallel. This also means that the integral of angular velocity does not yield the final orientation:

$$\int_0^t (\omega_1 + \omega_2) dt = \int_0^t (\omega_2 + \omega_1) dt \neq q(t) \tag{11}$$

This property has the potential to lead to a wide range of oculomotor accuracy problems. For example, it is known that the vestibular afferent signal generated by head movement driving the VOR is directly proportional to head angular velocity. Since the integral of angular velocity does not yield the final orientation, this signal can not be directly integrated to yield a desired eye position signal [31]. However, as can easily be appreciated in daily life, vision is stable with respect to the world regardless of the order in which head movements are executed, which indicates that the VOR is able to yield the correct eye position signal. The questions thus becomes how the angular velocity ω and the coordinate velocity \dot{q} are related. If we define the angular velocity vector as a quaternion with the scalar part zero and ω as the vectorial part, $\omega = (0, \omega)$, the answers are[18]:

$$\begin{aligned}
\dot{q}(t) &= \frac{\omega(t)q(t)}{2} \\
\omega(t) &= 2\dot{q}(t)q(t)^{-1}
\end{aligned} \tag{12}$$

We see here that the coordinate velocity not only depends on the angular velocity but also on the instantaneous eye position. Thus, in order to correctly integrate angular velocity to yield an accurate desired position a nonlinear multiplication with position is needed at some level of neural processing.

Since angular velocity is a vectorial quantity, it is the integral of angular acceleration. That is, if a (muscle) force generates a (rotational) torque (e.g. on the head), according to $\boldsymbol{\tau} = I\boldsymbol{\alpha}$, where I is the rigid body's moment of inertia (a 3x3 matrix), then the body's angular velocity is obtained from the time-integration of $\boldsymbol{\alpha}$:

$$\omega(t) = \int_0^t \boldsymbol{\alpha}(\tau) d\tau \rightarrow q(t) = \int_0^t \frac{\omega(\tau)q(\tau)}{2} d\tau \tag{13}$$

From Eqn. 10 it then follows that the relationship between the angular acceleration and the (changes in) orientation is given by

$$\ddot{q} = (\alpha q + \omega \dot{q})/2 = (\alpha q + (\omega)^2 q)/2 \rightarrow \alpha(t) = 2(\ddot{q}q^{-1} - (\dot{q}q^{-1})^2) \quad (14)$$

3.1.3 Using quaternions to describe 3D eye and head orientations

The goal of our model is to simulate 3-dimensional gaze shifts with a neurobiologically plausible scheme that includes the basic activity patterns of SC neurons. Gaze shifts are the result of the simultaneous rotations of the head with respect to the world, and of the eye with respect to the head. To this end we will use quaternions to describe the orientations, rotations and coordinate transformations required. The quaternion orientation is defined as the single axis rotation from the *primary position* to the current orientation, where the *primary position* defines straight ahead in the positive x-direction for the respective coordinate system. If $[1, 0, 0]$ is the vector corresponding to the primary direction, and $\hat{\mathbf{H}}$ is the unit vector describing the current pointing direction of the head's nose with respect to the world, then q_H is the quaternion such that:

$$\hat{\mathbf{H}} = q_H \circ [1, 0, 0] \circ q_H^{-1} \quad (15)$$

If $\hat{\mathbf{E}}$ is the unit vector pointing in the direction of the gaze line of the eye with respect to the head, then q_E is the quaternion, such that:

$$\hat{\mathbf{E}} = q_E \circ [1, 0, 0] \circ q_E^{-1} \quad (16)$$

$\hat{\mathbf{G}}$ is the unit vector pointing in the gaze direction, which is the orientation of the eye with respect to world and the result of, in that order, a rotation of the eye in the head and of the head on the neck. As a result the corresponding quaternion q_G becomes:

$$\begin{aligned} \hat{\mathbf{G}} &= q_H \circ \hat{\mathbf{E}} \circ q_H^{-1} \\ &= q_H \circ q_E \circ [1, 0, 0] \circ q_E^{-1} \circ q_H^{-1} \\ &= q_G \circ [1, 0, 0] \circ q_G^{-1} \end{aligned} \quad (17)$$

Thus, it is now possible to directly calculate the gaze orientation with respect to the primary position using:

$$q_G = q_H \circ q_E \quad (18)$$

As such, q_G , q_H and q_E are equivalent to $\hat{\mathbf{G}}$, $\hat{\mathbf{H}}$ and $\hat{\mathbf{E}}$ when describing the orientations of the gaze, head and eye. They can also be used to perform coordinate transforms between the world/body, head-on-neck and eye-in-head reference frames. When $\hat{\mathbf{E}}_T$ is the direction of a target relative to the eye as deduced from the position where light hits the retina and we want to know $\hat{\mathbf{H}}_T$, the direction of the target relative to head, we need to rotate the vector $\hat{\mathbf{E}}_T$ into the head reference frame. q_E is the rotation describing the orientation of the eye with respect to the head and as a result also describes the rotation that is needed to bring $\hat{\mathbf{E}}_T$ into the head reference frame:

$$\hat{\mathbf{H}}_T = q_E \circ \hat{\mathbf{E}}_T \circ q_E^{-1} \quad (19)$$

Similarly, if $\hat{\mathbf{G}}_T$ is the direction of the target with respect to the body the coordination transform between the head- and the body-centered reference frame is:

$$\hat{\mathbf{G}}_T = q_H \circ \hat{\mathbf{H}}_T \circ q_H^{-1} \quad (20)$$

The direction of the target with respect to the body can thus directly be derived from the oculocentric direction of the target using the orientation of the head-on-neck and the orientation of the eye-in-head:

$$\hat{\mathbf{G}}_T = q_H \circ q_E \circ \hat{\mathbf{E}}_T \circ q_E^{-1} \circ q_H^{-1} \quad (21)$$

This 3-D relationship between head orientation, eye-in-head orientation and gaze orientation will be used to build a quaternion model with separate head-on-neck and eye-in-head movement mechanisms, with the goal of achieving goal-directed and kinematically correct gaze shifts. Our model is heavily inspired by Tweed’s quaternion model [4]. In addition to Tweed’s model, as proposed by Van Opstal and Kasap[32][3], the gaze shift is driven by a dynamic desired (2D) gaze-velocity command which is encoded in the superior colliculus firing profile. Moreover, in contrast to the Tweed model, the eye- and head brainstem burst generators are assumed to be linear.

4 Model description

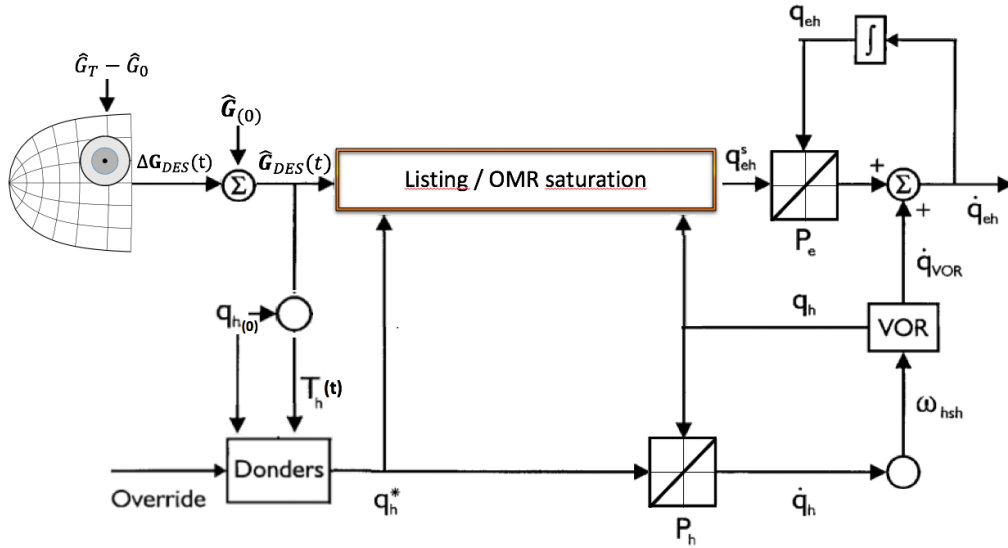


Figure 7: Schematic description of our model. The difference between the desired gaze direction $\hat{\mathbf{G}}_T$ and the initial gaze direction $\hat{\mathbf{G}}_0$ drives the SC (eq. 22). The integrated output of the SC determines the desired gaze displacement $\Delta \mathbf{G}_{DES}(t)$ (eq. 25) which is then added to the initial gaze direction $\hat{\mathbf{G}}_0$ to give the desired gaze direction in space $\hat{\mathbf{G}}_{DES}(t)$ (eq. 26). Combining $\hat{\mathbf{G}}_{DES}(t)$ and the initial orientation of the head q_{H_0} we find the direction of the target with respect to the head $\hat{\mathbf{H}}_T(t)$ (eq. 27), which is used to derive the desired orientation of the head q_h^* in the Donders’ box (eq. 28 to 31). The desired orientation of the head is combined with the desired direction in space in the Listing / OMR saturation box (the content of the box is identical to the content of the orange box in figure 6) to find the current desired OMR saturated orientation of the eye q_{eh}^s (eq. 33 to 37). The desired orientation of the head q_h^* is converted to a desired head coordinate velocity signal by the linear burst generator P_h and the saturated desired orientation of the eye is converted to a desired eye coordinate velocity by the linear burst generator P_e (eq. 41). The desired coordinate head velocity \dot{q}_h is converted to the head angular velocity ω_{hsh} which is used to derive the contribution of the VOR, \dot{q}_{VOR} to the eye velocity signal (eq. 42 and 43). \dot{q}_{VOR} is subsequently added to the desired eye velocity signal to obtain the final eye velocity signal \dot{q}_{eh} (eq. 44). Both the desired head and eye coordinate velocities are directly integrated using Euler’s method to obtain the updated eye and head orientations (eq. 45).

4.1 SC signal - desired gaze displacement in world coordinates

The superior colliculus programs the 2D desired gaze displacement in space. We will assume that prior to the SC any sensory information is transformed in to world coordinates using information about the orientation of the eye and the head at the moment of sensory stimulation, as shown in equation 21. If $\hat{\mathbf{G}}_0$ is a unit vector pointing in the direction of the gaze orientation in space prior to onset of movement (see equation 17), and $\hat{\mathbf{G}}_T$ is a unit vector pointing in the direction of the target in space (see equation 21), the difference between the two is:

$$\Delta \mathbf{G} = \hat{\mathbf{G}}_T - \hat{\mathbf{G}}_0 \quad (22)$$

We will assume this is the signal received by the SC and that with N_{spks} as the total number of spikes from the synchronised population burst, the subsequent SC motor signal per spike becomes:

$$\mathbf{M}_{SC} = \frac{\Delta \mathbf{G}}{N_{spks}} \quad (23)$$

We will simulate the firing profile of the SC by using a simplified rectangular pulse function $P(t)$ as used in the Kasap[32] model:

$$P(t) = \begin{cases} 0 & \text{for } t < 0 \text{ or } t > D \\ P & \text{for } 0 \leq t \leq D \\ \text{with } D = a \cdot \Delta G + b \text{ and } P = \frac{N_{spks}}{D} \text{ such that } P \cdot D \equiv N_{spks} \end{cases} \quad (24)$$

In this equation P is the firing rate in spikes/s, D the burst duration, in sec, and a (20 ms) and b (1.5 ms/°) are determined by the main-sequence amplitude-duration relation. This profile differs in its smoothness from more realistic, gamma-function-like SC burst profiles, but its decreasing amplitude and increasing duration for increasing gaze amplitudes simulates the most important properties thought to be responsible for main sequence behaviour. The output of the SC then becomes the instantaneous desired gaze displacement:

$$\Delta \mathbf{G}_{DES}(t) = \int_0^t \mathbf{M}_{SC} \cdot P(t) \cdot dt \quad (25)$$

This output is added to the initial gaze direction to obtain the dynamic desired gaze orientation. The x-component determining the length of the vector is fitted afterwards to yield a unit vector:

$$\begin{aligned} \mathbf{G}_{DES}(t) &= (\hat{\mathbf{G}}_0 + \Delta \mathbf{G}_{DES}(t))(\hat{\mathbf{y}} + \hat{\mathbf{z}}) \\ \hat{\mathbf{G}}_{DES}(t) &= [\sqrt{1 - (\mathbf{y}(t)^2 + \mathbf{z}(t)^2)}, \mathbf{y}(t), \mathbf{z}(t)] \end{aligned} \quad (26)$$

4.2 Desired orientation of the head

Head movement in gaze saccades is goal directed and strongly correlated to the initial head error. The dynamic head error vector with respect to the initial head orientation $q_{H(0)}^{-1}$ can be found by rotating the desired gaze direction into a craniocentric reference frame using the initial head orientation:

$$\hat{\mathbf{H}}_T(t) = q_{H(0)}^{-1} \circ \hat{\mathbf{G}}_{DES}(t) \circ q_{H(0)} \quad (27)$$

The rotation that would bring the head directly on goal if it would start in the primary direction, and roughly on goal if that is not case, is q_{HERR} :

$$q_{HERR}(t) = [\mathbf{1}, \mathbf{0}, \mathbf{0}] \rightarrow \hat{\mathbf{H}}_T(t) \quad (28)$$

The head only partially performs the gaze shift, with a horizontal contribution that is larger than the vertical contribution. Thus we rotate the head by a fraction of the complete head error. If $q_{HERR}(t) = q$:

$$q_{\Delta H}(t) = 0.5 \cdot q_y \circ \hat{\mathbf{j}} + 0.7 \cdot q_z \circ \hat{\mathbf{k}} \quad (29)$$

Next, the real of part $q_{\Delta H}(t)$ is fitted to yield a unit quaternion, which is then multiplied by that initial head orientation to obtain the desired head orientation:

$$q_{HDES}(t) = q_{H(0)} \circ q_{\Delta H}(t) \quad (30)$$

To obtain a result that fits Donders' law, the torsional component is fitted as a function of the horizontal and vertical components. If $q_{HDES} = q$

$$q_x = -0.15 \cdot q_y \circ q_z \circ \hat{\mathbf{i}} \quad (31)$$

The real part of q_{HDES} is then fitted to yield a unit quaternion. The 3D head motor error then becomes:

$$q_{HMOT-ERR}(t) = q_{HDES}(t) \circ q_{H(t)}^{-1} \quad (32)$$

4.3 Desired eye orientation in the head

We will derive the desired final eye orientation in the head by using the desired head orientation and the direction of the target in space. If we inversely rotate the desired gaze direction using the desired head orientation, we end up with the direction of the target with respect to the final head orientation.

$$\hat{\mathbf{H}}_{TDES}(t) = q_{HDES}(t)^{-1} \circ \hat{\mathbf{G}}_{DES}(t) \circ q_{HDES}(t) \quad (33)$$

If the final eye in head orientation would point in this direction when the head has reached its desired orientation, gaze would be on target. The desired final eye in head orientation then becomes the rotation from the primary direction to $\hat{\mathbf{H}}_{TDES}(t)$, which by definition does not have torsion and thus fits Listing's law:

$$q_{EF-DES}(t) = [\mathbf{1}, \mathbf{0}, \mathbf{0}] \rightarrow \hat{\mathbf{H}}_{TDES}(t) \quad (34)$$

Thus, the final desired gaze orientation becomes:

$$q_{GDES}(t) = q_{HDES}(t) \circ q_{EF-DES}(t) \quad (35)$$

In order to quickly get gaze on target, the eye in head orientation is not sent towards the final orientation of the eye in head, but directly towards the final gaze direction with respect to the current head orientation. The resulting current desired eye in head orientation then becomes:

$$q_{EC-DES}(t) = q_{H(t)}^{-1} \circ q_{GDES}(t) \quad (36)$$

In this way, gaze is quickly oriented towards the target and automatically ends up in Listing's plane when the head has reached its desired orientation. It is however limited by the oculomotor range (OMR), for which we will use the same procedure as in the '97 Tweed model, which is illustrated in figure 8. In short, if q_{EC-DES} has a larger deviation from the primary direction than 40° 's or a torsional component that is larger than 15° 's, which we assume is the range of the OMR, a line is drawn between the vectorial components of q_{EC-DES} and q_{EF-DES} , after which the new components are fitted on this line at the edge of the OMR.

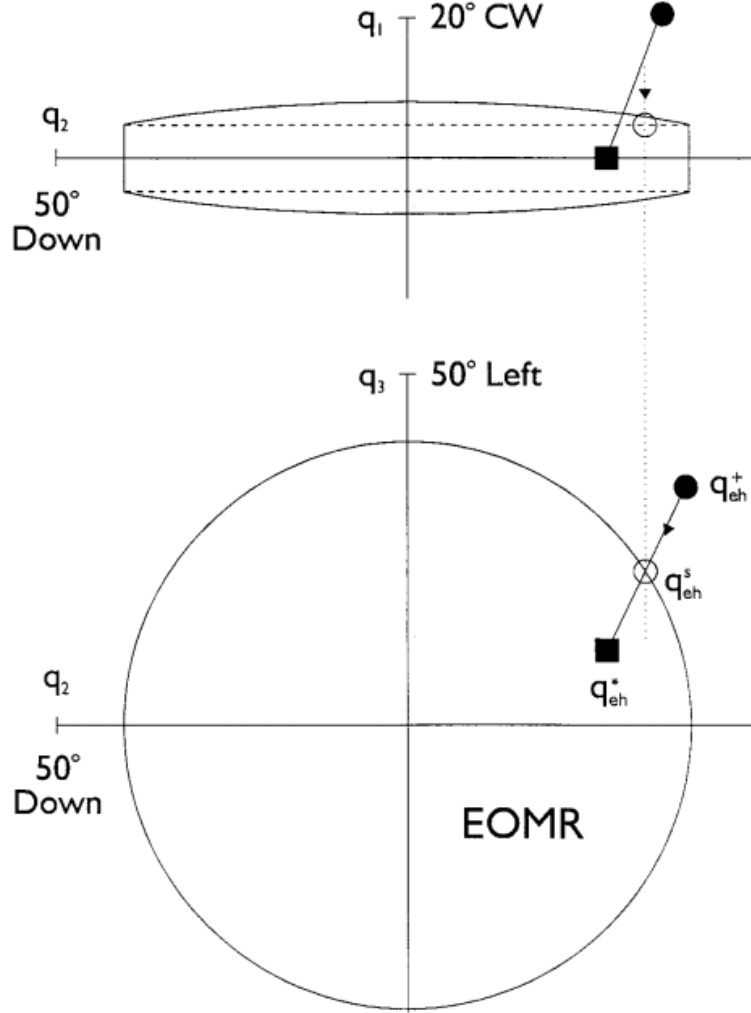


Figure 8: 3-dimensional OMR saturation, method and figure from '97 Tweed model[4]. A line is drawn between the vertical(q_2) and horizontal(q_3) rotational components of the current desired orientation (q_{eh}^+) and the final desired orientation (q_{eh}^*), after which the saturated desired vertical and horizontal components are fitted at the edge of the EOMR (effective oculomotor range). If the torsional components of this fit (q_1) is larger than the torsional EOMR, the torsional component is fitted such that it is within the torsional EOMR.

If we call the function that performs this saturation SAT , which takes the desired final and current eye-in-head orientation as input, the saturated desired orientation becomes:

$$q_{ES-DES}(t) = SAT([q_{EC-DES}(t), q_{EF-DES}(t)]) \quad (37)$$

The eye in head motor error then becomes:

$$q_{EMOT-ERR}(t) = q_{ES-DES}(t) \circ q_E^{-1}(t) \quad (38)$$

4.4 Linear eye and head burst generator

In the model, the linear burst generator creates a quaternion derivative from a motor error. The method is directly inspired by Tweed '97, with the difference that the gain is linear. The method uses

the relationship between the angular velocity and the quaternion derivative:

$$\dot{q} = \frac{\omega q}{2} \quad (39)$$

The vectorial part of the quaternion motor error is interpreted as a desired angular velocity and multiplied with the current orientation. If V_q is the function that takes the vector part of the quaternion, then:

$$\begin{aligned} \omega_{H_{DES}}(t) &= V_q(q_{H_{MOT-ERR}}(t)) \\ \omega_{E_{DES}}(t) &= V_q(q_{E_{MOT-ERR}}(t)) \end{aligned} \quad (40)$$

The resulting quaternion derivatives become, with the respective linear head and eye gains being G_H and G_E :

$$\begin{aligned} \dot{q}_H(t) &= G_H * \omega_{H_{DES}}(t) \circ q_H(t) \\ \dot{q}_{E_{DES}}(t) &= G_E * \omega_{E_{DES}}(t) \circ q_E(t) \end{aligned} \quad (41)$$

Eye and head movements do not always start at the same time, which are simulated in the model using delays where the difference between initial eye and head movement, $t_H(0) - t_E(0)$ is generated from a normal distribution (positive values indicate a head delay, see methods for mean and standard deviation). For head delays, G_H is set to zero for the duration of that delay and for eye delays G_E is set to zero for the duration of the delay.

4.5 VOR

The procedure in this paper is the same as in Tweed's model[4]. Depending on the size of the unsaturated eye-in-head motor error and the head angular velocity ω_H , which is directly computed from the head quaternion derivative $\dot{q}_H(t)$ and head orientation $q_H(t)$ using equation 39, a coordinate eye velocity is constructed:

$$\dot{q}_{VOR}(t) = \frac{(M * \omega_H) \circ q_E(t)}{2} \quad (42)$$

The factor M is a matrix which fully shuts off the contribution in the direction of the gaze motor error if the motor error is larger than 20°'s. Below 20°'s it is gradually turned on again. The procedure from Tweed's model[4] is as follows, where again V_q is the function that takes the vector part of the quaternion and A is the VOR shutoff amplitude of 20°'s.

$$\begin{aligned} x &= q_{EC-DES}(t) \cdot q_E^{-1}(t) ; \quad u = \frac{V_q(x)}{|V_q(x)|}; \quad C = \cos\left(\frac{A}{2}\right) \\ \text{If } x_0 &\leq C, \quad m = 1; \text{ else, } \quad m = \frac{1 - x_0}{1 - C}; \\ M &= m u u^T - I; \end{aligned} \quad (43)$$

Here, x is the unsaturated eye-in-head motor error and u is a vector containing the vector components of the eye-in-head motor error. If the motor error is zero, m is zero and M is equal to minus the 3x3 identity matrix I. As a result, the contribution of the VOR is precisely opposite the head angular velocity. When the real part of the motor error quaternion is smaller than C, the motor error is larger than 20°'s and the factor m becomes 1. The 3x3 matrix containing the vector components of the motor error, $u u^T$, is now completely added to M. As a result the contribution of the VOR is effectively shut-off in the direction of the motor error. If the motor error is between 20°'s and 0, the real part x_0 is between C and 1. Consequently, as the gaze error becomes smaller, the factor m goes becomes smaller and the VOR is gradually turned on in the direction of the gaze shift. The contribution is directly added to the eye quaternion derivative before integration. The final eye quaternion derivative then becomes

$$\dot{q}_E(t) = \dot{q}_{E_{DES}}(t) + \dot{q}_{VOR}(t) \quad (44)$$

4.6 Velocity integration

The quaternion derivatives for the eye and the head are integrated using Euler's method.

$$q(t + dt) = q(t) + \dot{q}(t) * dt \quad (45)$$

The quaternions are subsequently normalized to obtain unit quaternions:

$$q(t + dt) = \frac{q(t + dt)}{|q(t + dt)|} \quad (46)$$

The instantaneous 3D eye and head orientations are thus directly found by integrating the velocity signals, thereby ignoring the oculomotor plant which is not a part of our model.

5 Methods

5.1 Saccade parameters

The 3D orientations of the eye-in-the-head (q_E), head-on-neck (q_H) and gaze (q_G) are described using the torsional, vertical and horizontal rotational components, q_x , q_y and q_z from equation 1 respectively. In the figures where quaternion components q are plotted the axes are converted to degrees using the approximation:

$$^\circ \approx 2 \cdot \arcsin(q) \quad (47)$$

The directions of the eye-in-the-head ($\hat{\mathbf{E}}$), head-on-neck ($\hat{\mathbf{H}}$), gaze ($\hat{\mathbf{G}}$) ($\hat{\mathbf{T}}$) relative to the primary position and the directions of the targets relative to the eye, head and gaze directions are described using the azimuth (horizontal displacement) and elevation (vertical displacement) in a double polar coordinate system[33]. The eccentricity (R) and angle with respect to the horizon (ϕ) of a vector $[x, y, z]$ are given by:

$$\begin{aligned} R &= \arcsin(\sqrt{y^2 + z^2}) \\ \phi &= \arctan\left(\frac{z}{y}\right) \end{aligned} \quad (48)$$

The azimuth (A) and elevation (E) in a double polar coordinate system relate to these angles in the following way:

$$\begin{aligned} A &= \arcsin(\sin R \cdot \cos \phi) \\ E &= \arcsin(\sin R \cdot \sin \phi) \end{aligned} \quad (49)$$

The azimuthal, elevational and total shift (E, H or G) displacement are defined as follows:

$$\begin{aligned} \Delta AZ &= AZ(end) - AZ(0) \\ \Delta EL &= El(end) - EL(0) \\ \Delta SHIFT &= \sqrt{\Delta AZ^2 + \Delta EL^2} \end{aligned} \quad (50)$$

The end points for the gaze and head shift are defined at the final time points of the trial. The eye shift however, as can be seen in figure 2 (see E_{END}), is over while the head is still moving. We will estimate the end of the contribution of the eye shift to the gaze shift by defining it at the last time point where the contribution in the direction of the desired eye orientation ($\dot{q}_{E_{DES}}$) is larger than the contribution of the VOR (\dot{q}_{VOR}) to the eye shift (see equation 44). Note that this does not mean that

\dot{q}_{EDES} and \dot{q}_{VOR} are zero. The relative contributions of the eye (CE) and the head (CH) to the gaze shift are now defined as:

$$CE = \frac{\Delta E}{\Delta G}$$

$$CH = \frac{\Delta H}{\Delta G}$$
(51)

Angular velocities are approximated using:

$$\begin{aligned} \delta AZ &= AZ(t+1) - AZ(t) \\ \delta EL &= EL(t+1) - EL(t) \\ \omega &\approx \sqrt{\delta AZ^2 + \delta EL^2} \end{aligned}$$
(52)

To determine the influence of the initial eye ($\hat{\mathbf{E}}_T$) and head ($\hat{\mathbf{H}}_T$) error, or Target-re-Eye and Target-re-Head respectively, on the head displacement, multiple linear regression was performed on equation 53 using the 'regress' function in Matlab.

$$\begin{aligned} \Delta H_{AZ} &= a \cdot \hat{\mathbf{H}}_T^{AZ} + b \cdot \hat{\mathbf{E}}_T^{AZ} + c \\ \Delta H_{EL} &= d \cdot \hat{\mathbf{H}}_T^{EL} + e \cdot \hat{\mathbf{E}}_T^{EL} + f \end{aligned}$$
(53)

5.2 Model parameters

Each time step dt in the model consists of 1 ms and the duration of each trial was 0.8 s. The linear gain for the velocity burst generator for eye movements, G_E , is 30. The gain for head movements, G_H , is 8 (see equation 41). These have been fitted using a visual inspection of the data in order to roughly visually resemble data in human subjects and have not been computationally optimized.

5.3 Experiment parameters

To test the performance and behaviour of our model we simulated multiple experiments with different parameters. The goal of each experiment and the parameters that were used are described below.

5.3.1 Traces of oblique gaze shifts

In order to test whether our model is able to replicate basic properties of gaze shifts we simulated gaze shifts to four targets at $R = [50]^\circ$ and $\phi = [45, 110, 210, 300]^\circ$ with a duration of 0.6 seconds. The initial eye and head orientation were centered and thus aligned. Eye and head latency delays were randomly generated with a mean of 25 ms and a standard deviation of 5 ms (positive values indicate a delay of head movement).

5.3.2 Consecutive targets

To test whether our model could simulate gaze shifts consecutive targets where an accumulation of torsion was a potential problem we simulated gaze shifts to six targets where the initial orientation of the eye and the head before the gaze shift to the next target was given by the final orientation of the gaze shift to the previous target. The initial orientation was centered. The targets had eccentricities of 60° , except the final one which was set at zero. The angles with respect to the horizon ϕ changed with 90° every time to form a square and where in order: $[135, 225, 315, 45, 135, 0]^\circ$. No eye and head latency delays were used for this simulation.

5.3.3 Gaze shifts with unaligned initial head and gaze orientations

Gaze shifts where the initial eye and head orientation were unaligned revealed that head movements are directed toward the initial head error and not towards the initial eye error[8]. We wanted to see whether our model could replicate the results of this experiment, thus we simulated a very similar experiment. The experiment had 500 trials with randomly generated targets with eccentricities between 0° and 50° and angles with respect to the horizon ϕ between 0° and 360° . The initial orientation of the head had randomly generated initial vertical and horizontal rotational components between -25° and 25° . In half of the trials the eye-in-the-head orientation was centered in its primary position causing the head and gaze orientation to be aligned. In the other half of the trials the orientation of the eye-in-the-head was precisely opposite that of the head such that the initial gaze orientation was centered and unaligned with the head orientation. Initial torsional rotational components were always zero. In the aligned condition the initial eye error (Target-re-Eye) and initial head error (Target-re-Head) are identical, while in the unaligned condition they differ. Delays were randomly generated with a mean of 70 ms and a standard deviation of 20 ms (positive values indicate a delay of head movement). This experiment was also performed on Tweed’s model, whose code was provided in his paper[4]. Eye and head latency delays were not present in Tweed’s model and were therefore also excluded in this simulation.

5.3.4 Gaze shifts with random initial orientations and random targets

To test the kinematics of our model where we wanted to see if our model could replicate main sequence properties we simulated trials with random initial eye and head orientations and random target directions. The simulation had 1000 trials with randomly generated targets with eccentricities between 0° and 60° and angles with respect to the horizon ϕ between 0° and 360° . The initial orientation of the head had randomly generated initial vertical and horizontal rotational components between -30° and 30° and the initial torsional component was set at $0.15 \cdot |q_y| \cdot |q_z|$ to fit torsional orientations seen in human subjects[22]. The initial orientation of the eye-in-the-head had randomly generated initial vertical and horizontal rotational components between -25° and 25° , while the initial torsional component was always zero in order to fit Listing’s plane. Delays were randomly generated with a mean of 70 ms and a standard deviation of 20 ms (positive values indicate a delay of head movement). This experiment was also performed on Tweed’s model, whose code was provided in his paper[4]. Eye and head latency delays were not present in Tweed’s model and were therefore also excluded in this simulation.

5.3.5 Gaze shifts with centered initial orientations to targets within the OMR

The analysis of the relative contribution of the eye versus the latency difference between eye and head movement in the trials with random initial orientations and random target directions seemed to suggest there was not a correlation. We wanted to test whether the OMR limiting eye movement was the reason for this apparent lack of correlation and thus we simulated 500 trials to targets within the OMR. Targets were randomly generated with eccentricities between 20° and 40° and angles with respect to the horizon between 0° and 360° . The initial orientations of the eye and the head were always centered. Delays were randomly generated with a mean of 70 ms and a standard deviation of 40 ms. (positive values indicate a delay of head movement).

6 Results

6.1 Traces of oblique gaze shifts

In order to test whether the model is able to reproduce basic fundamental properties of combined eye plus head gaze shifts we simulated four gaze shifts to oblique targets where both the eye and the head

are initially in the primary orientation looking straight ahead. On the left of figure 9 we see that for each horizontal and vertical direction gaze is goal directed and follows an almost straight line. Head movement is towards but not directly aimed at the target and the eye moves towards the target up until the moment it starts moving in the opposite direction of the head as a result of the VOR. On the right of figure 9 we see that the torsional component of the eye deviates from listing plane during the movement but returns to it at the end of movement, whilst the torsional component of the head keeps increasing with eccentricity.

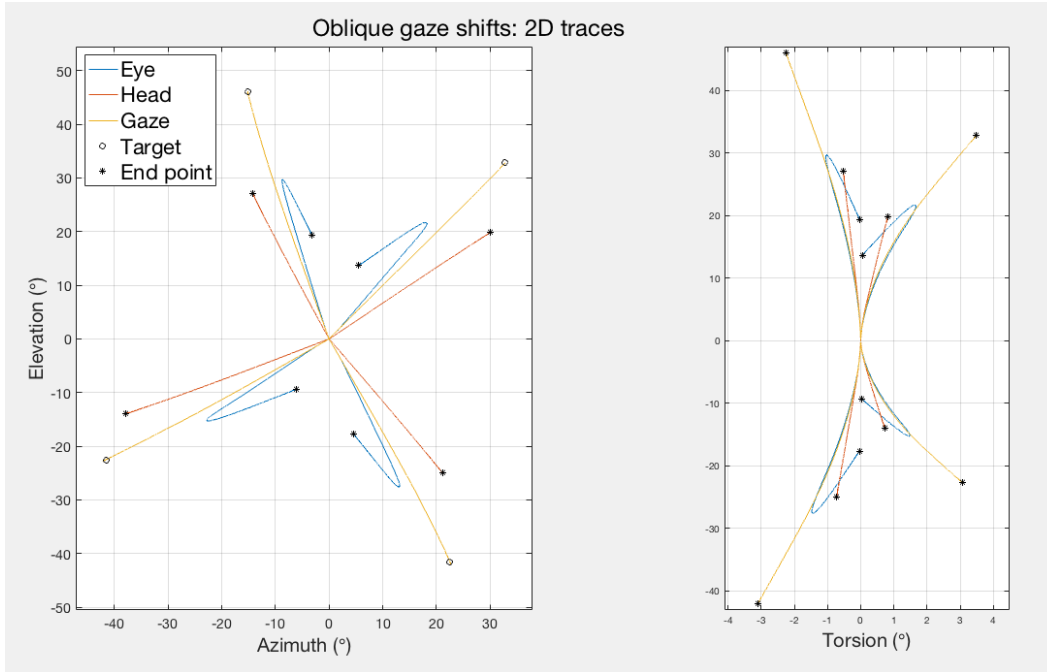


Figure 9: 2D-traces of the eye, head and gaze of four oblique gaze shifts. **Left:** Azimuthal and elevational traces of the eye, head and gaze. Gaze is successfully directed at the target at the end of the gaze shift and all traces move towards their targets except for the eye which moves in the opposite direction of the head in the latter part of the gaze shift as a result of the VOR. **Right:** Elevational and torsional traces of the eye, head and gaze. The torsional component of the gaze and head increase with eccentricity, while the eye returns to the zero torsion plane at the end of each gaze shift. Note the difference in scale with the left figure.

In figure 10 we can inspect the kinematics of these oblique gaze shifts, where we can note the similarities with figure 2. Eye movement is faster than head movement and moves back with opposite but equal velocity after the eye shift whilst the head is still moving towards the target. Gaze moves towards the target and is stable in space as soon as the target is acquired while the head and eye are still moving. In contrast to figure 2 the end of the gaze shift does not coincide with the end of the eye shift, but is a bit later. Achieving better synchronization in the model probably require at least precisely optimized parameters which are not present in the current model.

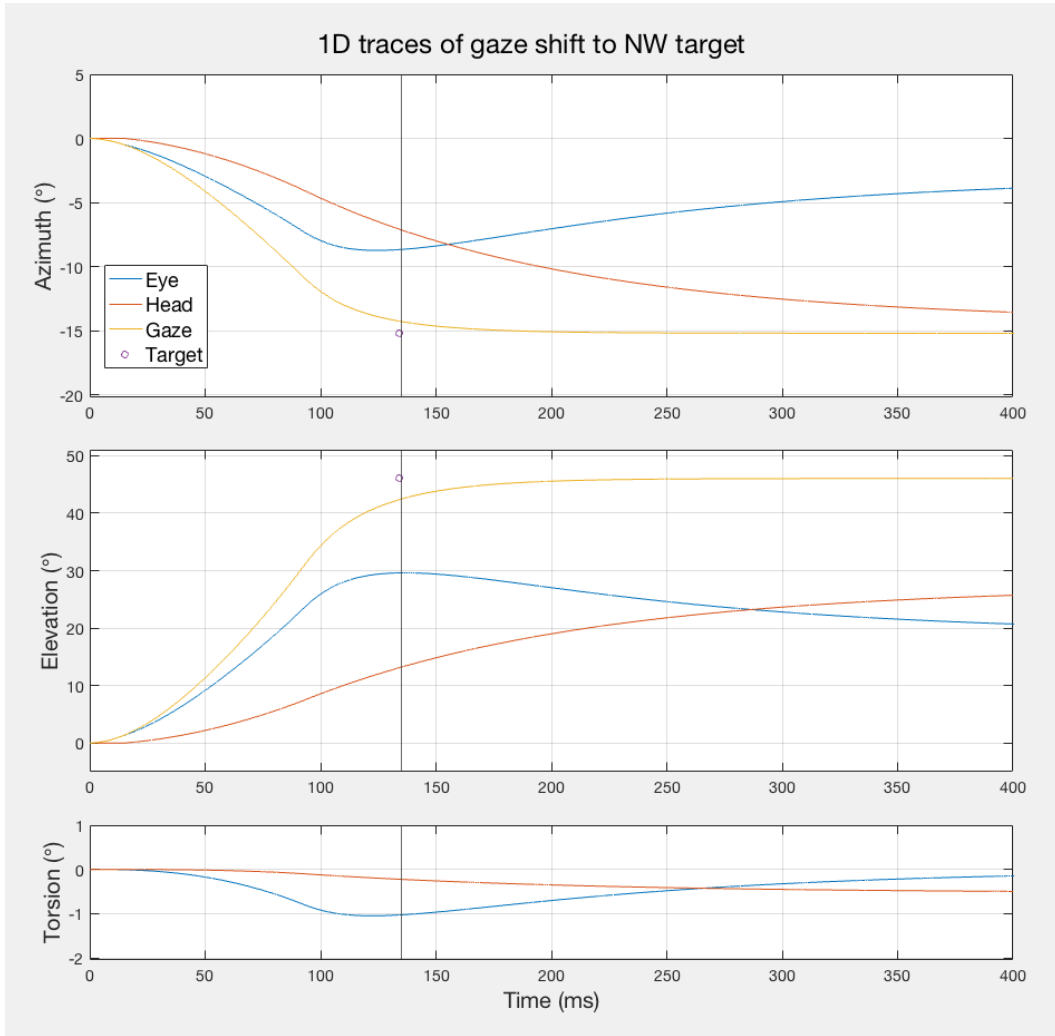


Figure 10: 1D traces of the eye, head and gaze during the gaze shift to the northwest target in figure 9. The vertical black line indicates the end of contribution of the eye to the gaze shift (see Saccade parameters). **Top:** Azimuthal trace. Gaze, head and eye all move in the direction of the target, except for the eye which moves in the opposite direction of the head as a result of the VOR as soon as gaze close to the target. **Mid:** Elevational trace. Gaze, head and eye all move in the direction of the target, except for the eye which moves in the opposite direction of the head as a result of the VOR as soon as gaze close to the target. **Bottom:** Torsional trace of the head and the eye during the gaze shift. Torsion of the eye increases in the first part of the gaze shift, but slowly returns to zero as a result of the VOR in the latter part. The torsional component of the head keeps increasing while the azimuthal and elevational component of the keep increasing. Note the differences in scale between the subplots

6.2 Consecutive targets

In figure 11 and 12 we can see how the model executes consecutive gaze shifts from the origin to an eccentric target, between eccentric targets and back to the origin. We want to see whether the model is able to take the initial 3D orientation of the eye and the head into account and successfully direct gaze at the target. Furthermore we want to see if the consecutive 3D rotations lead to an accumulation

of torsion, a potential problem with 3D rotations for eye-head gaze shifts. The 2D gaze trajectories in figure 11 show that gaze is indeed always directed at the target and its trace forms a rectangular shape. The oblique saccades to and from the origin are perfectly straight and the horizontal and vertical saccades are almost perfectly straight. The subtle deviations of the gaze trajectory from a perfect straight line between eccentric targets are similar to the predictions of the Tweed model and data observed in human subjects[34]. The trace of the 2D head trajectory does not form a square however but is rather shaped like a parallelogram. Its movement is directed towards the initial head error and for each gaze shift starting in an eccentric position the head error has both a horizontal and vertical component. The resulting head shift will therefore also be oblique. This differs from the predictions of the Tweed model and data observed in human subjects[34], where the 2D traces of the head follow a rectangular shape for these consecutive gaze shifts. In the Tweed model head movement is directed towards the direction of the target in space and thus, if the targets in space are shaped in the form of a rectangle, head movements traces will be rectangular. In our model head movement is directed towards the initial head error as head displacement is strongly correlated with the head error[8]. Further implications of this difference will be discussed in more detail below. In addition, we see in figure 11 that head displacements after eccentric initial head orientations seems to overshoot the target, most notably horizontally, while the rotation is supposed to be only a fraction of the initial head error. However, if the head starts in the primary orientation (like the first saccade starting in the origin of the figure) the resulting head movement is indeed a fraction of the initial head error with a larger horizontal than vertical contribution. This is an indication that the method used to derive the desired head rotation becomes worse when initial eccentricity increases. In figure 12 we can see the 3D eye, head and gaze orientations during the consecutive gaze shifts. In the top row we can see the components of horizontal and vertical rotation axes describing vertical and horizontal rotation respectively. For the eye we can see that that rotation follows almost a straight line and reverses direction near the end of the shift as a result of the VOR. The gaze and head horizontal and vertical rotation components follow the shape of the 2D traces in figure 11, where for the head we can note the larger components on the vertical axis with respect to the horizontal axis. This indicates, as expected, larger horizontal than vertical displacements. In the lower row of figure 12 we can inspect the torsional components of the orientation. For the eye in the head we can see clear deviations from the zero torsion axis, Listing's plane, of a few degrees during the gaze shift, but the final orientations are always back in Listing's plane (not always clearly visible). The head also has small deviations from the zero torsion plane, which is expected as it is supposed to be a function of the horizontal component multiplied with the vertical component, $q_y \circ q_z$.

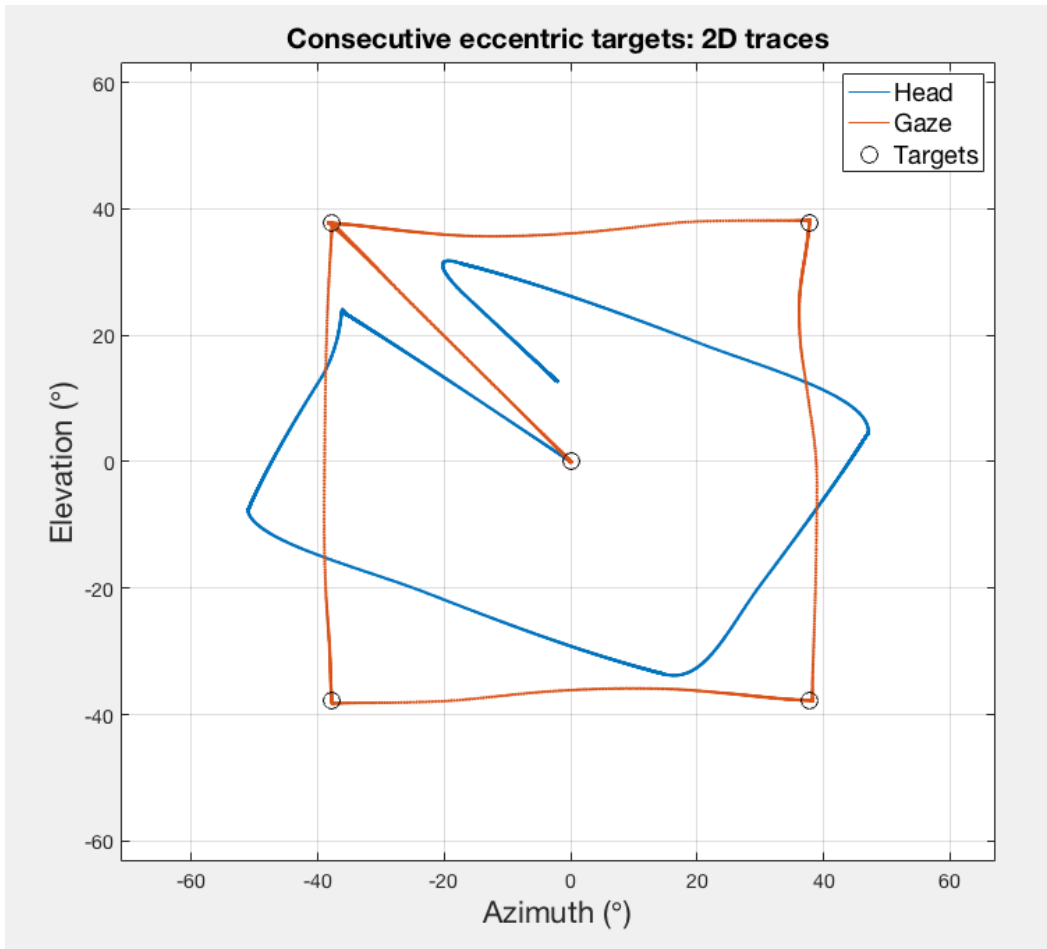


Figure 11: 2D traces of the azimuthal and elevational components of six consecutive gaze shifts (counterclockwise). Gaze movement is goal directed for each gaze shift. Head movements are also goal directed with a larger horizontal than vertical displacement but tend to overshoot the desired target especially in the horizontal direction.

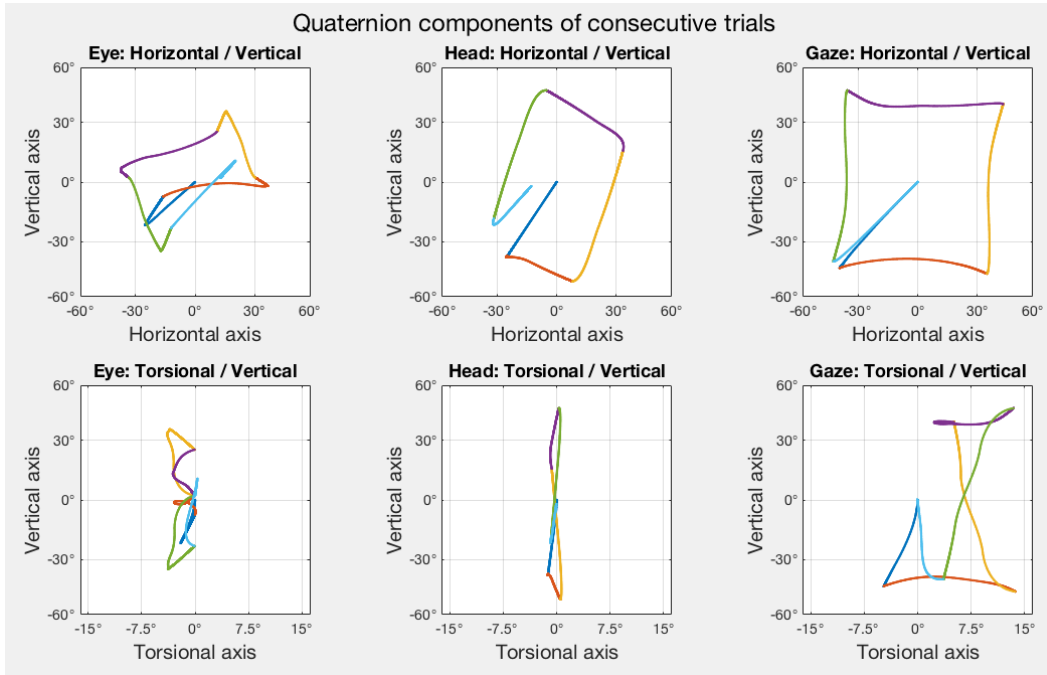


Figure 12: 3D rotational quaternion components of the consecutive gaze shifts in figure 11. **Top:** Vertical and horizontal rotational components. **Bottom:** Vertical and torsional rotational components. **Left:** Eye rotational components. The change of direction as a result of the VOR can clearly be noted in the top figure, while in the bottom figure we see that the eye deviates from Listing’s plane during the gaze shift. **Mid:** Head rotational components. The top figure resembles a rotated version of the head trace seen in figure 11, while in the bottom we see small deviations from the zero torsion plane. **Right:** Gaze rotational components. The top figure resembles a rotated version of the gaze trace seen in figure 11 and in the bottom we see large deviations from the zero torsion plane.

6.3 Gaze shifts with unaligned initial head and gaze orientation

Head displacement in human subjects is strongly correlated with the initial head error (Target-re-Head) and not with the initial eye error (Target-re-Eye), as shown in experiments where the initial head and eye orientation are either aligned or unaligned in order to be able to differentiate between the eye and head error.[8]. Therefore in our model the desired head rotation is derived from the initial head error. To confirm whether our model is able to replicate the results seen in human subjects a comparable experiment was done with our model. Targets were chosen randomly and the initial head orientation was also chosen randomly. The eye-in-head is either rotated with the head and still in the primary position (aligned) or counter-rotated in precisely the opposite direction such that the gaze is centered (unaligned). In the aligned condition Target-re-Head and Target-re-Eye are identical, while in the unaligned condition they are not. The azimuthal and elevational head displacement as a function of the Target-re-Head and Target-re-Eye can be found in figure 13. In the left part of figure 13 we see that in both the aligned and unaligned conditions the head displacement seems linearly scaled with the head error, with a stronger scaling for the azimuthal displacement. This is expected, as the desired vertical rotation is scaled smaller than the horizontal rotation in the model to simulate head displacement measurements in human subjects. In the right part of figure 13 we see the head displacement with respect to the Target-re-Eye. In the aligned condition, where the Target-re-Eye and the Target-re-Head are identical, head displacement and Target-re-Eye also seem linearly scaled. In the unaligned condition however the displacement scatters around the aligned results, suggesting it might not be linearly scaled. To test these assumptions we performed multiple

linear regression analysis on equation 53 to find the contributions of the head and eye error to the horizontal and vertical displacement components. The results are shown in equation 55, where we see that there is a significant correlation between the Target-re-Head and the final head displacement, with a stronger scaling in the horizontal direction. The correlation between Target-re-Eye and the head displacement is insignificant for both the horizontal and the vertical displacements. Consequently our model replicates the results that inspired Goossens’ model[8] with very similar figures and multiple linear regression results.

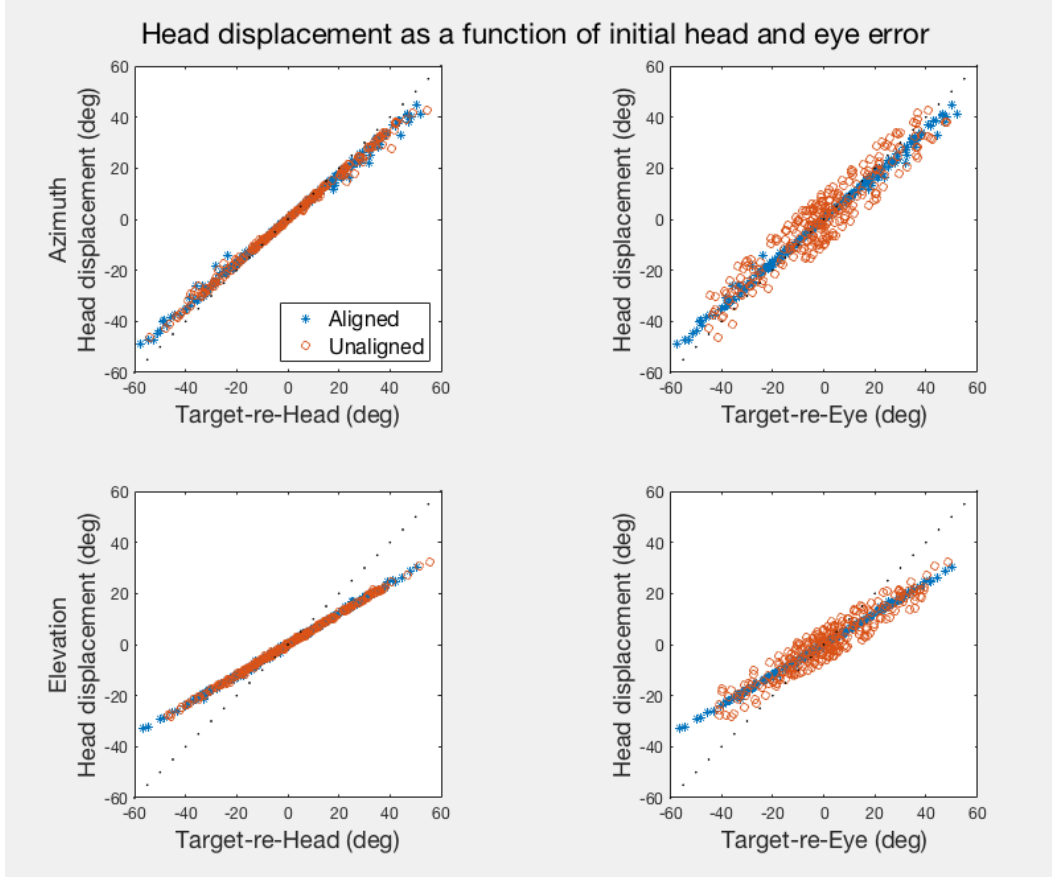


Figure 13: Head displacement as a function of initial head and eye motor error. Eye and head motor error are either aligned (blue) or unaligned (orange). **Left:** Head motor error. both the horizontal (top) and vertical (bottom) are strongly correlated to the initial head motor error in both the aligned and unaligned conditions, with a larger horizontal correlation. **Right:** Eye motor error. For both the horizontal (top) and vertical (bottom) displacements the head displacement is strongly correlated to the eye motor error in the aligned condition, but looks much more scattered in the unaligned condition. Multiple linear regression analysis (see equation 55) confirms that head displacement is strongly correlated to the initial head motor error and not to the initial eye motor error.

Multiple linear regression was performed using the following equations:

$$\begin{aligned} \Delta H_{AZ} &= a \cdot \hat{\mathbf{H}}_T^{AZ} + b \cdot \hat{\mathbf{E}}_T^{AZ} + c \\ \Delta H_{EL} &= d \cdot \hat{\mathbf{H}}_T^{EL} + e \cdot \hat{\mathbf{E}}_T^{EL} + f \end{aligned} \quad (54)$$

The result is shown below. Offsets were close (mean smaller than 0.03 and standard deviation around

0.1) and are thus not shown.

$$\begin{aligned}\Delta H_{AZ} &= 0.83 \pm 0.02 \cdot T_{h^{AZ}} + 0.03 \pm 0.02 \cdot T_{e^{AZ}} \\ \Delta H_{EL} &= 0.61 \pm 0.01 \cdot T_{h^{EL}} + -0.01 \pm 0.01 \cdot T_{e^{EL}}\end{aligned}\tag{55}$$

To compare our model with the Tweed model we performed the exact same experiment with the original Tweed model. The results are shown in figure 14. On the left part of the figure we see that in both the aligned and unaligned conditions the relation between the Target-re-Head and the head displacement looks much more scattered than in figure 13. The azimuthal head displacement with respect to the Target-re-Eye in the upper right looks similar to figure 13, the elevation in the lower right looks very scattered in both conditions however. The multiple linear regression analysis of equation 53 on the Tweed model has the following results:

$$\begin{aligned}\Delta H_{AZ} &= -0.63 \pm 0.04 \cdot T_{h^{AZ}} + 1.51 \pm 0.04 \cdot T_{e^{AZ}} + 0.13 \pm 0.27 \\ \Delta H_{EL} &= -0.92 \pm 0.02 \cdot T_{h^{EL}} + 1.22 \pm 0.02 \cdot T_{e^{EL}} + 0.02 \pm 0.11\end{aligned}\tag{56}$$

In this experiment for the head displacement there seems to be a strong negative correlation with the Target-re-Head and a strong positive correlation with the Target-re-Eye and the offsets are no longer close to zero. The Tweed model thus clearly does not replicate the findings of Goossens[8]. This is expected as the head displacement is not directed towards the initial head error but only depends on the orientation of the target in space, irrespective of the initial eye and head error.

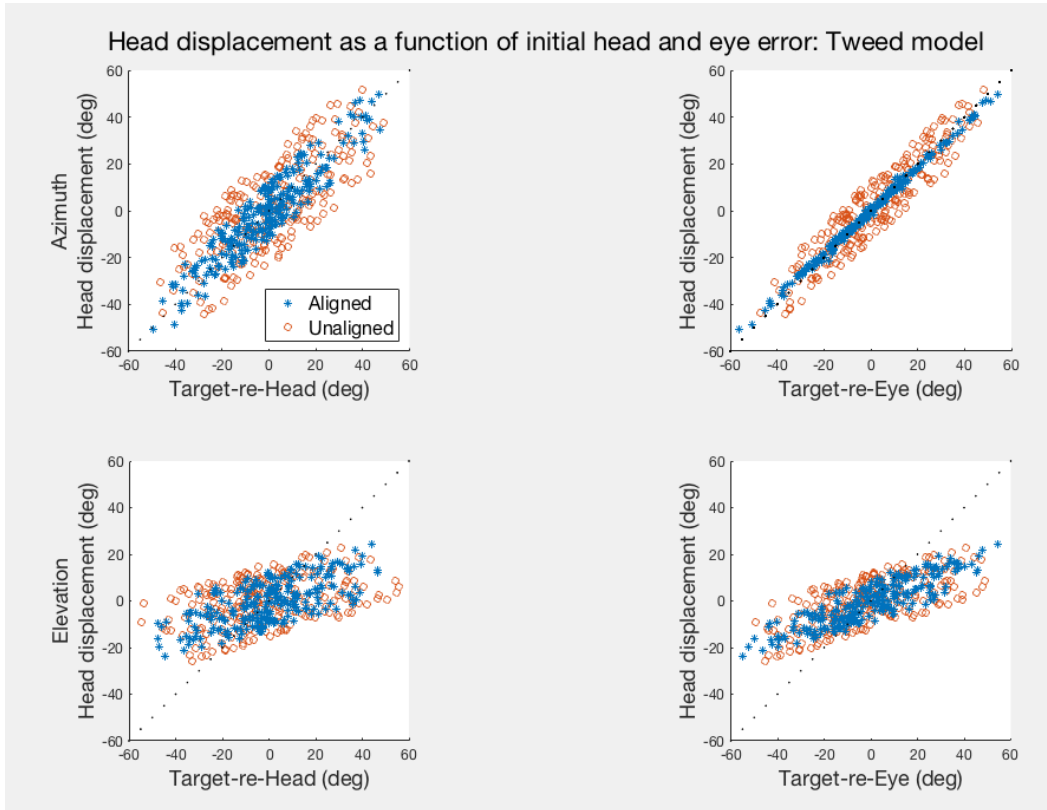


Figure 14: Head displacement as a function of initial head and eye motor error in the Tweed model. Both the horizontal (**top**) and vertical (**bottom**) displacements do not seem tightly correlated to the initial head motor error (**left**) or the initial eye motor error (**right**) in either the aligned (blue) or unaligned (orange) conditions, except for the aligned condition in the top right figure. Both the figure and the MLR result in equation 56 illustrate the dissimilarity of Tweed’s model with our model

6.4 Trials with random initial orientation and random targets

To test the kinematics of our model we simulated trials with random initial eye and head orientation and random targets. The rotational quaternion components of all orientations during these trials are shown in figure 15. In the upper row we see the horizontal and vertical rotational components, where the eye orientations form a circle and the head orientations an oval with larger vertical rotations (horizontal displacements) than horizontal rotations (vertical displacements). In the lower row we see the torsional components. The eye clearly deviates from Listing’s plane during the gaze shift. The standard deviation from Listing’s plane is 0.4° and the deviation seems to be smaller for smaller eccentricities. The mean and standard deviation of the end points are practically zero (data not shown), which does not replicate typical reported standard deviations of around 1° [35]. As our model does not have any form of noise or uncertainty in the velocity generation this is expected. The head also deviates from the zero torsion plane similarly to the Tweed model and the data it is based on[34].

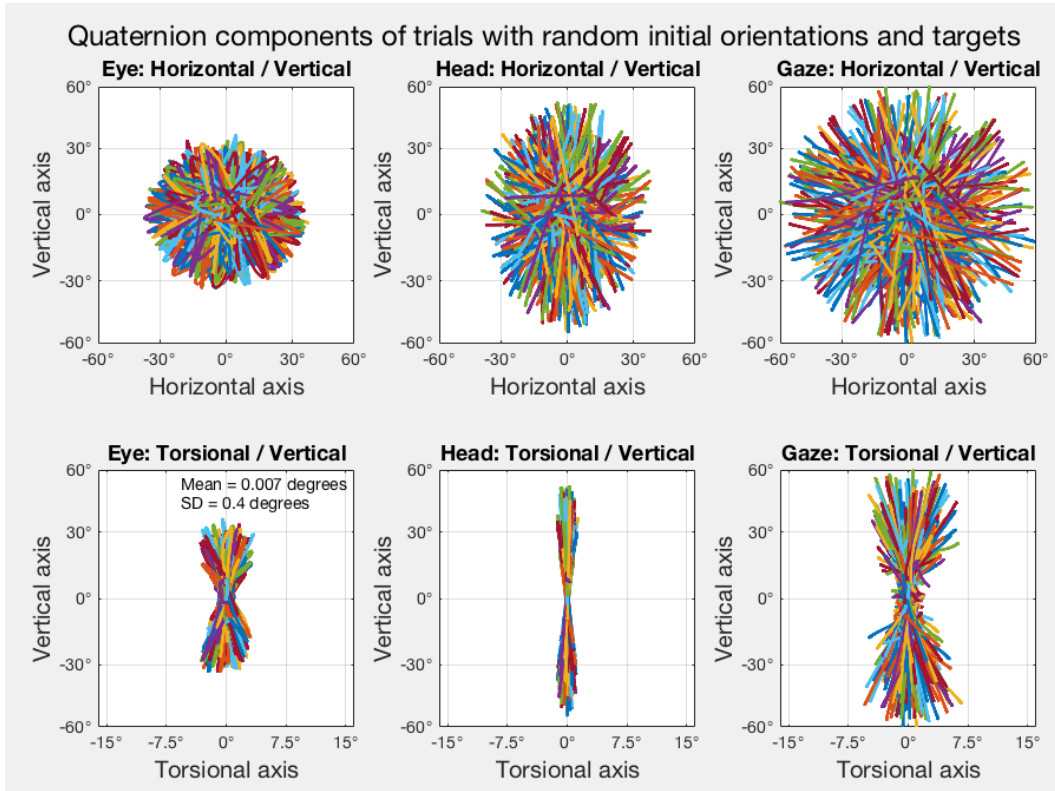


Figure 15: 3D rotational quaternion components of all data points of all trials with random initial orientations and random target directions. **Top:** Horizontal and vertical components. **Bottom:** Vertical and torsional rotational components. **Left:** Eye rotational components. Horizontal and vertical components are in all directions, but are limited at the OMR (40°). The torsional components show clear deviations from Listing’s plane during the gaze shift. **Mid:** Head rotational components. Horizontal and vertical components are in all directions with larger components on the vertical than on the horizontal axis. Small deviations from the zero torsion plane can be seen in the lower figure. **Right:** Gaze rotational components. Gaze is oriented in all directions horizontally and vertically and large torsional components can be noted in the lower figure

We performed the exact same experiment with the Tweed model and plotted all data points of all trials, the results are shown in figure 16. Here we can see that the results are very similar, but the horizontal and vertical components of the eye and the head are more oval-shaped with respect to figure 15. This likely caused by the difference in the definition of the desired head movement, which in the Tweed model is defined as a fraction of the spatial error with a larger horizontal (vertical axis) than vertical (horizontal axis) contribution. This is precisely the shape we see in the figure. As the eye movement is always fitted such that the target is acquired, its shape in the figure conforms to the shape of the head movements. This likely causes in both figure 15 and 16 for the horizontal and vertical components of the eye to resemble an inverted shape of the horizontal and vertical components of the head.

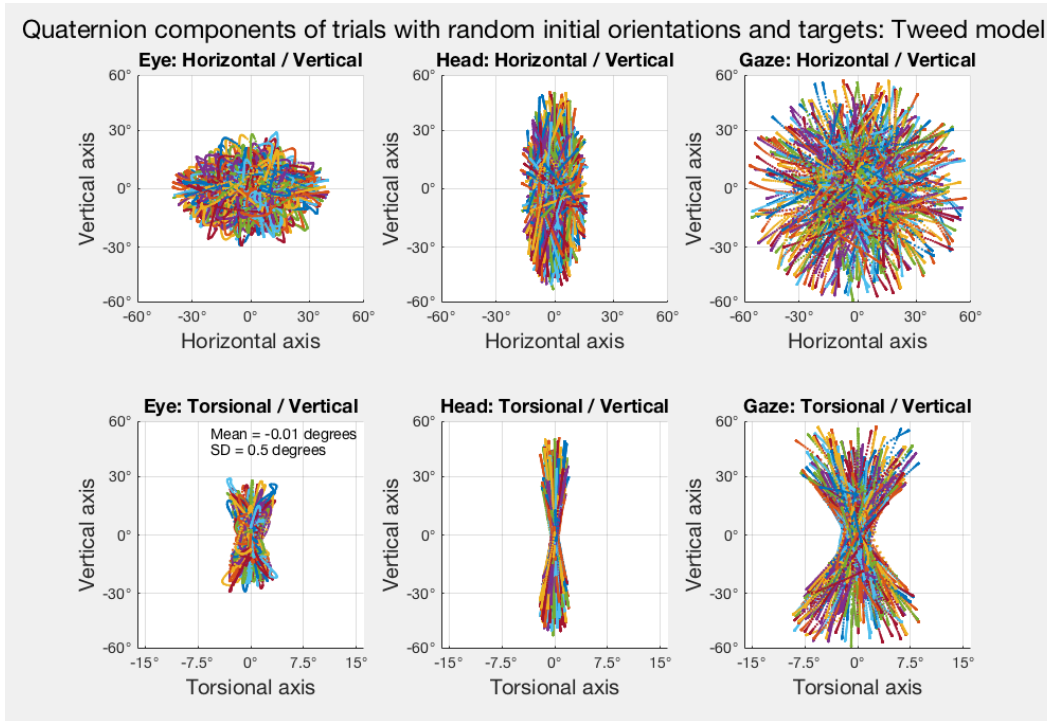


Figure 16: 3D rotational quaternion components of the Tweed model of all data points of all trials with random initial orientations and random target directions. The figure shows great similarity to figure 15. **Top:** Horizontal and vertical components. **Bottom:** Vertical and torsional rotational components. **Left:** Eye rotational components. Horizontal and vertical components are in all directions, but are limited at the OMR (40°). Larger horizontal than vertical components can be noted in this experiment. The torsional components show clear deviations from Listing's plane during the gaze shift. **Mid:** Head rotational components. Horizontal and vertical components are in all directions with larger components on the vertical than on the horizontal axis. Small deviations from the zero torsion plane can be seen in the lower figure. **Right:** Gaze rotational components. Gaze is oriented in all directions horizontally and vertically and large torsional components can be noted in the lower figure

One of the main goals our model is to create a three dimensional model where the firing properties of the SC explain the main sequence of saccades while the velocity burst generators remain linear. An important property of the main sequence is saturating peak eye and gaze velocities for saccades of increasing amplitudes. Thus we analyzed the peak velocities for all the random trials and the results are plotted in figure 17. There we see that for the gaze, eye and head the velocities indeed saturate, indicating our model can simulate main sequence behaviour. The effect is however not as strong as it is in human subjects. This can possibly be explained by the rectangular function used to describe the firing properties of the SC, which is only a simple approximation of actual firing properties. The effect is even smaller for the peak head velocity in our model, which is likely due to the latency delays of head movements negating the effect of SC firing on the peak velocity.

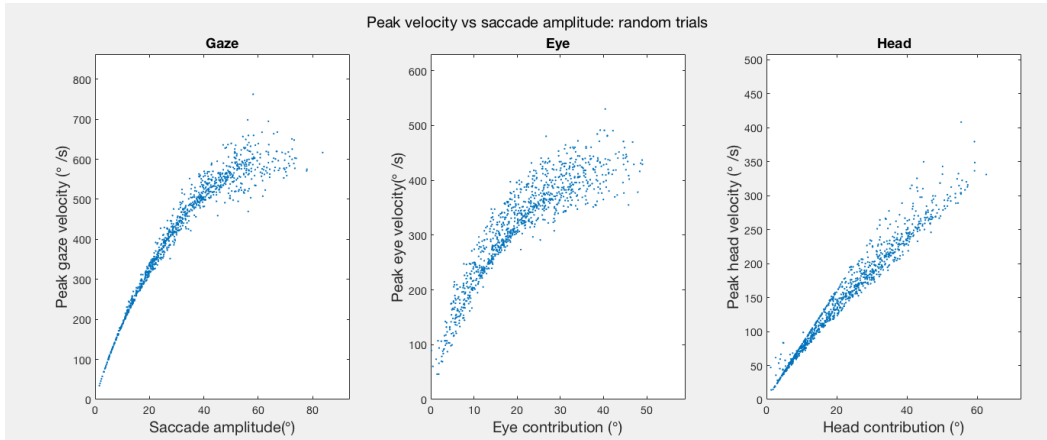


Figure 17: Analysis of saccade kinematics of all random trials. Peak gaze (**left**), eye (**mid**) and head (**right**) velocities are plotted against the saccade amplitude, eye contribution and head contribution respectively. Both the peak gaze and eye velocities clearly saturate with increasing amplitudes. Head velocities seem to saturate less strongly and part of the data does not seem to saturate. Scatter of the data is likely caused by random eye and head latency delays and by the OMR limiting eye movement in a subset of the data.

6.5 Gaze shifts to targets within the OMR

Using the data from the experiment with random initial orientations and target directions the relative eye and head contributions were plotted against the head-eye latency difference. The figure (not shown) resembled a random scatter plot, suggesting there was not any correlation. The total head displacement only depends on the initial head error, so the lack of correlation for the relative head contribution is expected. Eye movement however is always goal directed, so for delayed head movement a larger relative contribution of the eye is expected. In trials with a large head-eye latency a high relative eye contribution is expected. In trials where the opposite occurred, a large head-eye latency difference and a low relative eye contribution, visual inspection of movement traces seemed to suggest eye movement might be limited by the oculomotor range. This was tested in trials where the OMR was not a limiting factor and the results are shown in figure 18. In this figure we now see a clear increase in the relative eye contribution for increasing head-eye latency, confirming that the eye is indeed goal directed while the head is not moving and reproducing data in human subjects[8]. The relative head contribution versus the head-eye latency difference still resembles a random scatter plot, which is expected as the head contribution still only depends on the initial head error and not on the initial eye-in-head orientation. This also does not replicate findings in human subjects as relative head contribution tends to decrease with increased head-eye latency[8].

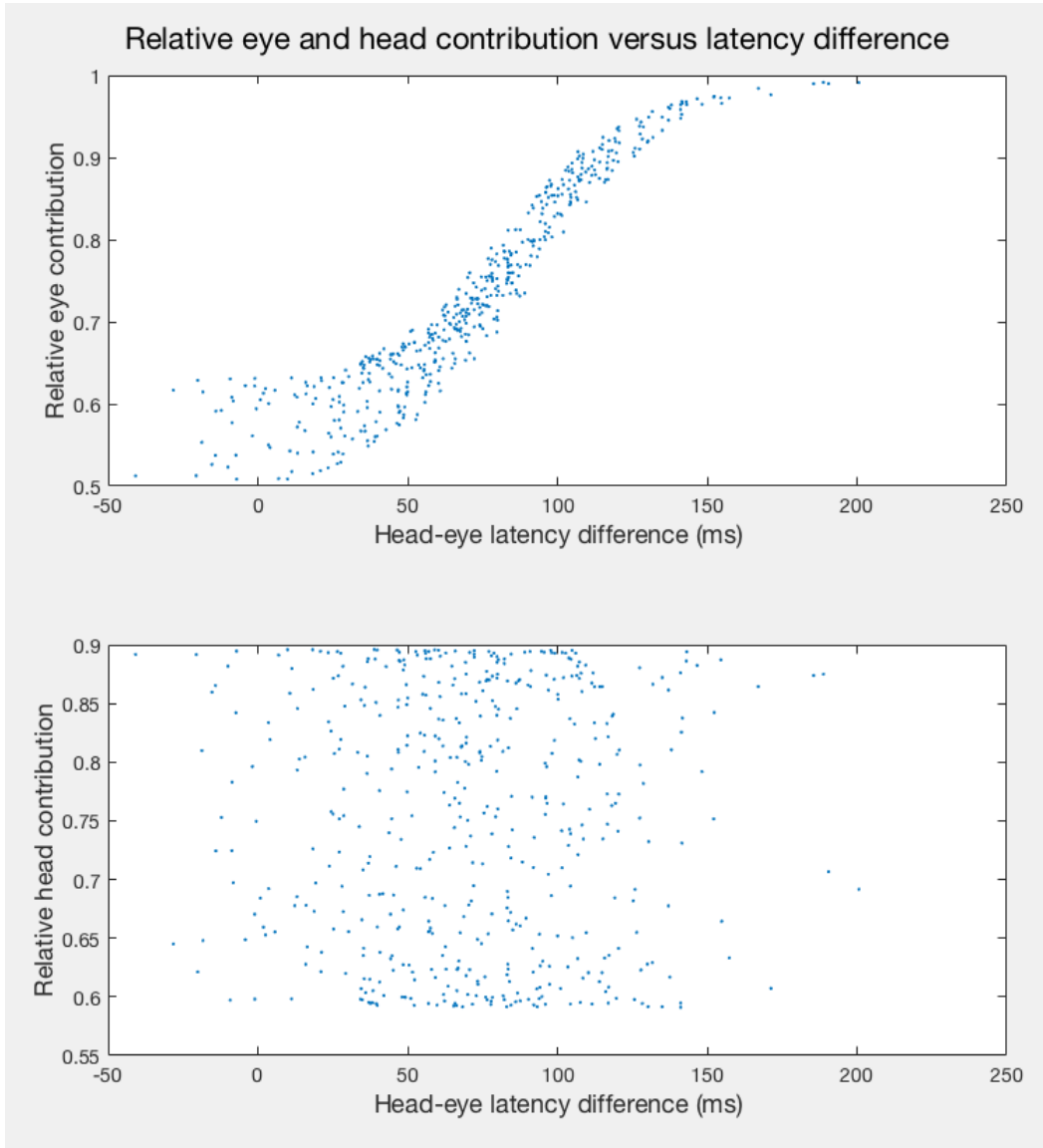


Figure 18: The relative contribution of the eye (**top**) and the relative contribution of the head (**bottom**) as a function of the latency difference between the eye and the head for trials that all start at the origin with targets that are all within the OMR. A positive latency difference indicates a delay of head movement. The relative contribution of the eye seems to increase sigmoidally with increasing latency difference. The relative contribution of the head does not seem related at all to the latency difference and resembles a random scatter plot. The limits of the relative head contribution are only determined by the direction of the head displacement with larger horizontal than vertical displacements.

7 Discussion

The goal of the model was to simulate 3D eye-head gaze shifts with a neurobiologically plausible scheme that incorporates recent findings about the role of the SC and has linear velocity burst generators that is able to replicate important characteristics of gaze shifts. This has been proven successful.

Movements traces of the eye, head and gaze are very similar to gaze shifts in human subjects (see figure 9 and 10) and consecutive gaze shifts are equally accurate and do not result in an accumulation of torsion (see figure 11). In gaze shifts with combined eye and head movements the torsional components of the eye deviate from Listing’s plane during the gaze shifts but return to it at the end of the head movement (see figure 9, 10 12), as is the case with gaze shifts in human subjects. Furthermore, head movements have larger horizontal than vertical contributions (see figure 13) and equation 55) and are directed towards the initial head error (see equation 55). In figure 11 we can also note however that head movements do tend to overshoot the target in gaze shifts with large eccentricities, indicating that the method of deriving the desired head orientation requires improvement. The relative contribution of the eye increases with the head-eye latency difference (see figure 18) similarly to gaze shifts in humans and confirms that eye movements are goal directed irrespective of head movement. However, this is only found in gaze shifts where the eye is not limited by the OMR. The head-eye latency difference has been shown to depend on the initial eye position[3], but in our model the head-eye latency difference is randomly generated. Thus, the relative head contribution in our model only depends on the relative direction (horizontal/vertical) of the initial head error and our model does not replicate the decreasing contribution with increasing head-eye latency difference found in human gaze shifts. The most important conclusion is that our 3D model, in which the kinematics are determined by the firing properties of the SC and the velocity burst generators are linear, has saturating peak velocities for increasing amplitudes (see figure 17). This makes it the first 3D model that is able to reproduce main sequence properties with linear burst generators and it shows that it is possible to create a 3D model with linear burst generators that is able to make realistic gaze shifts and shows main sequence characteristics.

This also marks the biggest conceptual difference with the Tweed model, in which the SC signal is interpreted as a step function and the burst generators are nonlinear in order to get main sequence properties. The desired final gaze orientation $\hat{\mathbf{G}}_T$ is the same as in Tweed’s model (T_S in his model description), which are both derived using equation 21. In our model however the current desired gaze orientation, $\hat{\mathbf{G}}_{DES}(t)$ is dynamic and brought towards $\hat{\mathbf{G}}_T$ with the SC firing rate determining the velocity in which $\hat{\mathbf{G}}_{DES}(t)$ is brought from $\hat{\mathbf{G}}_0$ to $\hat{\mathbf{G}}_T$. Another big difference between our model and the Tweed model is the way the desired orientation of the head is determined. In Tweed’s model, the desired orientation is solely based on the direction of the target in space irrespective initial orientation of the head. As head movement is directed towards the initial head error[8], the desired orientation of the head in our model is derived from the initial head error. The consequence of this difference can clearly be noted in figures 13 (our model) and 14 (Tweeds model) and in the corresponding multiple linear regression analysis (respectively equation 55 and 56). These show that, in contrast to Tweed’s model, head movement in our model is indeed directed towards the initial head error. The other parts of the model, with the exception of the velocity burst generators which are linear in our model, are identical between Tweed’s and our model. These are the method of deriving the desired orientation of the eye in the head and how it ends up in Listing’s plane, the method of saturating the desired current orientation of the eye in the head at the OMR and the implementation of the VOR.

Our model has therefore adapted parts of the Tweed model and gave it an explicit role for the SC and head movement that better replicate data[8][1][2], but there are still parts that require improvement. In figure 11 it can clearly be noted that the head movement overshoots the target in the azimuthal direction. The head is supposed to rotate a fraction of the initial head error. Rotating more would be non-optimal from both a duration and energy conservation perspective. Thus, the current method of deriving the desired head rotation is flawed and does not correctly determine the required rotation. As the first of the consecutive head movements seems to be quite accurate and only the head movements with large initial head eccentricities are not, the initial eccentricity of the head is the likely cause of inaccuracy.

A possible solution would be to firstly determine a desired direction instead of a desired rotation, similarly to the derivation of $\hat{\mathbf{G}}_{DES}(t)$ in equation 22. To achieve this we would first determine the difference between the desired direction of gaze and the initial direction of the head (in essence, the initial head error): $H_{ERR}(t) = \hat{\mathbf{G}}_{DES}(t) - \hat{\mathbf{H}}(0)$. Subsequently the horizontal and vertical components of this difference are then scaled to give larger horizontal than vertical contributions and added to $\hat{\mathbf{H}}(0)$ and fitted in the same manner as equation 26 to obtain $\hat{\mathbf{H}}_{DES}(t)$. The desired 3D orientation, $q_{H_{DES}}$ is then fitted at this direction to conform to Donders' law. Only now the desired rotation is determined, which is done by deriving the motor error (see equation 32). Another improvement in the model would be the inclusion of strategies that optimize the way the model deals with the OMR. Currently the eye is limited at the OMR, but this has no further consequence in terms of movement strategies. As a result, the eye is often limited at the OMR especially when the delay of the head is relatively large. If we had plotted the data from the trials with random initial orientations and random targets (see figure 15) in figure 18, the increase of the relative eye contribution with increasing head delay would no longer be present. Only when the trials are chosen such that the OMR is never a limiting factor, as is done with the trials in figure 18, the increase of relative eye contribution is revealed.

Currently in the model, the delay is randomly generated from a uniform distribution and the relative head contribution is only dependent on whether the displacement is horizontal (larger contribution) or vertical (smaller contribution). In human subjects, the eye-head latency difference, the relative head contribution and the firing profile of the SC is dependent on the initial eye position such that in cases where the OMR could be a limiting factor the delay of the head is shorter, the contribution of the head is larger, the firing rate of the SC burst is lower and the duration of the burst is longer[3]. According to our proposed role of the SC in kinematics where the firing rate encodes the desired gaze velocity, this could reveal a neural strategy of dealing with the limits of the OMR. If a target is presented that is in the direction of the limits of the OMR, the strategy would be to start head movement relatively early (lower delay for the head) and to lower the velocity of the desired gaze displacement and increase its duration (higher burst velocity and increased burst duration, respectively) to slow down the combined eye and head movement, therefore preventing the relatively fast moving eye from being limited at the OMR. Implementing the eye position dependent delay and SC profiles to see whether this results in movement strategies that conform to what is seen in human subjects would thus be a good potential improvement for the model.

In addition, implementing more realistic SC burst profiles that resemble what is found in SC measurements to see how this affects the main sequence properties would also be an interesting subject of study for the model. A crucial point of discussion is that our model currently does not implement the oculomotor plant, which transforms the velocity signals from the burst generator into desired position signals for the muscles. In our model we have assumed that the axes of rotation are orthogonal and that the primary positions of the eye and head perfectly coincide with looking straight ahead to the horizon, as these assumptions tremendously simplify the required mathematics. However, both assumptions are known to be incorrect. Muscles are not arranged orthogonally and the primary direction of the eye is not parallel to the horizontal plane, making the generation of appropriate velocity signals and the implementation of Listing's and Donders' law significantly less trivial than it currently is in our model. We believe that is possible to neurally control torsion and have thus implemented this as such in our model, but the alternative to the neural model proposes that ocular torsion is controlled mechanically through the muscles in a pulley-like system. Although we do not believe this can completely explain eye movement behaviour like how the eye ends up in Listing's plane precisely at the end of the head displacement as a result of the VOR, the method in which ocular muscles control eye position at a detailed level is still poorly understood and leaves a lot of room for modulation. In fact, a study providing a detailed eye plant model incorporating realistic muscle mechanics found that purely passive mechanic control is impossible and will result in drift while at the same time concluding

that a pulley-like system is probably necessary in order to keep the muscles stable in the globe[36]. Thus, studying the oculomotor plant and the ocular muscles is an important task for the future if we want to better understand gaze shifts.

It is also interesting to note that in our model we have assumed that both the eye and the head have saturating peak velocities for increasing saccade amplitudes as their kinematics equally depend on the SC firing profiles. Saturating peak velocities for the eye are well documented, but the kinematics of the head less so. Further studies of head kinematics are therefore useful to confirm or refute this assumption.

Furthermore, in our model the head can not translate with respect to the body and the body does not translate with respect to the world. Both assumptions are clearly not true and accurately combining 3D translations and rotations would greatly complicate the model even further. It is therefore clear that the challenge of creating a complete 3D model of gaze shifts is far from over and further studies in the oculomotor field are required in order realize this.

8 Conclusion

We have successfully created the first 3D gaze shift model with combined eye and head movements where the kinematics are determined by the superior colliculus firing profiles, therefore proving it is theoretically possible to do so. The model does not yet include oculomotor plant mechanics and translations of the body and the head during gaze shifts and further neurobiological, psychophysical and computational studies are required in order to incorporate these.

References

- [1] HHLM Goossens and AJ Van Opstal. Dynamic ensemble coding of saccades in the monkey superior colliculus. *Journal of Neurophysiology*, 95:2326–2341, 2006.
- [2] HHLM Goossens and AJ van Opstal. Optimal control of saccades by spatial-temporal activity patterns in the monkey superior colliculus. *PLoS Comput Biol*, 8(5):e1002508, 2012.
- [3] AJ van Opstal and B Kasap. Maps and sensorimotor transformations for eye-head gaze shifts: Role of the midbrain superior colliculus. In *Progress in brain research*, volume 249, pages 19–33. Elsevier, 2019.
- [4] D Tweed. Three-dimensional model of the human eye-head saccadic system. *Journal of Neurophysiology*, 77(2):654–666, 1997.
- [5] AT Bahill, MR Clark, and L Stark. The main sequence, a tool for studying human eye movements. *Mathematical biosciences*, 24(3-4):191–204, 1975.
- [6] MF Jay and DL Sparks. Sensorimotor integration in the primate superior colliculus. i. motor convergence. *Journal of neurophysiology*, 57(1):22–34, 1987.
- [7] DA Robinson. Eye movements evoked by collicular stimulation in the alert monkey. *Vision research*, 12(11):1795–1808, 1972.
- [8] HHLM Goossens and AJ Van Opstal. Human eye-head coordination in two dimensions under different sensorimotor conditions. *Experimental Brain Research*, 114(3):542–560, 1997.
- [9] JD Crawford and D Guitton. Visual-motor transformations required for accurate and kinematically correct saccades. *Journal of Neurophysiology*, 78:1447–1467, 1997.

- [10] R Jürgens, W Becker, and HH Kornhuber. Natural and drug-induced variations of velocity and duration of human saccadic eye movements: evidence for a control of the neural pulse generator by local feedback. *Biological cybernetics*, 39(2):87–96, 1981.
- [11] JA Van Gisbergen, DA Robinson, and S Gielen. A quantitative analysis of generation of saccadic eye movements by burst neurons. *Journal of Neurophysiology*, 45(3):417–442, 1981.
- [12] A Roucoux, D Guitton, and M Crommelinck. Stimulation of the superior colliculus in the alert cat. *Experimental Brain Research*, 39(1):75–85, 1980.
- [13] EG Freedman, TR Stanford, and DL Sparks. Combined eye-head gaze shifts produced by electrical stimulation of the superior colliculus in rhesus monkeys. *Journal of neurophysiology*, 76(2):927–952, 1996.
- [14] C Fernandez and JM Goldberg. Physiology of peripheral neurons innervating semicircular canals of the squirrel monkey. ii. response to sinusoidal stimulation and dynamics of peripheral vestibular system. *Journal of neurophysiology*, 34(4):661–675, 1971.
- [15] CC Barr, LW Schultheis, and DA Robinson. Voluntary, non-visual control of the human vestibulo-ocular reflex. *Acta oto-laryngologica*, 81(5-6):365–375, 1976.
- [16] VP Laurutis and DA Robinson. The vestibulo-ocular reflex during human saccadic eye movements. *The Journal of Physiology*, 373(1):209–233, 1986.
- [17] AA Kardamakis and AK Moschovakis. Optimal control of gaze shifts. *Journal of Neuroscience*, 29(24):7723–7730, 2009.
- [18] D Tweed and T Vilis. Implications of rotational kinematics for the oculomotor system in three dimensions. *Journal of Neurophysiology*, 58(4):832–849, 1987.
- [19] T Haslwanter. Mathematics of three-dimensional eye rotations. *Vision research*, 35(12):1727–1739, 1995.
- [20] FC Donders et al. *Holländische Beiträge zu den anatomischen und physiologischen Wissenschaften*, volume 1. Bötticher, 1848.
- [21] D Tweed, W Cadera, and T Vilis. Computing three-dimensional eye position quaternions and eye velocity from search coil signals. *Vision research*, 30(1):97–110, 1990.
- [22] B Glenn and T Vilis. Violations of listing’s law after large eye and head gaze shifts. *Journal of Neurophysiology*, 68(1):309–318, 1992.
- [23] D Straumann, Th Haslwanter, M-C Hepp-Reymond, and K Hepp. Listing’s law for eye, head and arm movements and their synergistic control. *Experimental Brain Research*, 86(1):209–215, 1991.
- [24] M Ceylan, DYP Henriques, DB Tweed, and JD Crawford. Task-dependent constraints in motor control: pinhole goggles make the head move like an eye. *Journal of Neuroscience*, 20(7):2719–2730, 2000.
- [25] FF Ghasia and DE Angelaki. Do motoneurons encode the noncommutativity of ocular rotations? *Neuron*, 47(2):281–293, 2005.
- [26] D Guitton and M Volle. Gaze control in humans: eye-head coordination during orienting movements to targets within and beyond the oculomotor range. *Journal of neurophysiology*, 58(3):427–459, 1987.

- [27] H Misslisch, D Tweed, and T Vilis. Neural constraints on eye motion in human eye-head saccades. *Journal of Neurophysiology*, 79(2):859–869, 1998.
- [28] AJ Van Opstal, K Hepp, Y Suzuki, and V Henn. Role of monkey nucleus reticularis tegmenti pontis in the stabilization of listing’s plane. *Journal of Neuroscience*, 16(22):7284–7296, 1996.
- [29] D Tweed, T Haslwanter, and M Fetter. Optimizing gaze control in three dimensions. *Science*, 281(5381):1363–1365, 1998.
- [30] M Daemi and JD Crawford. A kinematic model for 3-d head-free gaze-shifts. *Frontiers in computational neuroscience*, 9:72, 2015.
- [31] DB Tweed, TP Haslwanter, V Happe, and M Fetter. Non-commutativity in the brain. *Nature*, 399(6733):261–263, 1999.
- [32] B Kasap and AJ Van Opstal. Modeling auditory-visual evoked eye-head gaze shifts in dynamic multisteps. *Journal of neurophysiology*, 119(5):1795–1808, 2018.
- [33] EI Knudsen, GG Blasdel, and M Konishi. Sound localization by the barn owl (*tyto alba*) measured with the search coil technique. *Journal of comparative physiology*, 133(1):1–11, 1979.
- [34] D Tweed, B Glenn, and T Vilis. Eye-head coordination during large gaze shifts. *Journal of neurophysiology*, 73(2):766–779, 1995.
- [35] AJ van Opstal, K Hepp, BJ Hess, D Straumann, and V Henn. Two-rather than three-dimensional representation of saccades in monkey superior colliculus. *Science*, 252(5010):1313–1315, 1991.
- [36] C Quaia and LM Optican. Three-dimensional rotations of the eye. *Adler’s physiology of the eye: clinical application*. New York: Mosby, pages 818–29, 2003.

9 Data figures

The model and the scripts required to replicate the data and figures can be found in the map '3Dgaze-model.Lennaert'. In order to replicate an experiment and generate the corresponding figures, simply run the corresponding script (see below) from the folder 'experiments'. These scripts also contain the experiment parameters and can be edited there. The 'quaternion' toolbox, which is contained in the 'biofysica' toolbox is required to run the scripts.

The execution (running the model with the relevant parameters) and the analysis (e.g. convert to azimuth / elevation) are done by the 'runandanalyze' scripts which can be found in the 'execute_and_analyze' folder.

Plotting of the data is done by the 'plotexperiments' scripts which can be found in the 'plotfigures' folder.

The script of our model is called 'threeDgaze' and can be found in the 'Model.Lennaert' folder. Tweed's model can be found in the 'Model.Tweed' folder.

Figure 9 and 10 Script used to generate figures: figure1.m
Analysis can be edited in Runandanalyze.m
Figures can be edited in plotexperiments_figure1.m

Figure 11 and 12 Script used to generate figures: figure2.m
Analysis can be edited in Runandanalyze_consecutivetargets.m
Figures can be edited in plotexperiments_figure2.m

Figure 13 Script used to generate figure: figure3.m
Analysis can be edited in Runandanalyze.m
Figures can be edited in plotexperiments_figure3.m

figure 14 Script used to generate figure: testtweedaligned.m
Analysis can be edited in runandanalyzeandplot_tweed97.m
Figures can be edited in plottweedaligned

figure 15 and 17 Script used to generate figures: figure4.m
Analysis can be edited in Runandanalyze.m
Figures can be edited in plotexperiments_figure4.m

figure 16 Script used to generate figure: testtweedrandomtrials.m
Analysis can be edited in runandanalyzeandplot_tweed97_randomtrials.m
Figures can be edited in plottweed.m

figure 18 Script used to generate figure: figure5.m
Analysis can be edited in Runandanalyze.m
Figure can be edited in plotexperiments_figure5.m